Mathematisches Forschungsinstitut Oberwolfach

Report No. 5/2005

Gemischte und nicht-standard Finite-Elemente-Methoden mit Anwendungen

Organised by
Dietrich Braess (RU Bochum)
Carsten Carstensen (HU Berlin)
Klaus Hackl (RU Bochum)

January 30th – February 5th, 2005

ABSTRACT. Mixed and non-conforming finite element methods form a general mathematical framework for the spatial discretisation of partial differential equations, mainly applied to elliptic equations of second order and are becoming increasingly important for the solution of nonlinear problems. These methods are under active discussion in the mathematical and the engineering community and aim of the workshop was to provide a joint forum for the current state of research.

Introduction by the Organisers

Mixed finite element methods (MFEM) form a general mathematical framework for the spatial discretisation of partial differential equations, mainly applied to elliptic equations of second order. They become increasingly important for the solution of nonlinear problems. In contrast to standard finite element schemes the mixed finite element discretisation of problems in divergence form, i.e. $f + \operatorname{div} \sigma = 0$ where $\sigma = A(\nabla u)$, $\sigma \in L$ and $u \in H$, allows more flexibility in the design of the discrete approximation spaces contained in L and H, i.e. in the spaces for the direct variables and the Lagrange multipliers.

The workshop focuses on new developments in the field of mixed and non-standard finite element methods. The main points are

- The analysis of mixed FE formulations and of non-conforming methods, including, for instance, enhanced strain and discontinuous Galerkin methods, cf. (F. Armero), (D. Braess), (R. Durán), (K. Garikipati), (P. Monk), (F. Radu), (D. Reddy), (S. Reese), (R. Sacco), (J. Schöberl), (W. Wagner), (R. Winther), (B. Wohlmuth).

- The effective and reliable error estimation of finite element methods as the basis for adaptive techniques and error control, cf. (M. Ainsworth), (P. Houston) and (R. Rannacher).
- Numerical techniques to handle strong and weak discontinuities predicted by the underlying boundary value problem, cf. (P. Steinmann). Cracks and material failure need to be simulated in accordance with the physical experiment, cf. (P. Hansbo), (U. Hoppe), (K. Weinberg).
- For a range of phenomena in structural mechanics the microscale of the material needs to be taken into account to obtain accurate numerical solutions, cf. (T. Arbogast).

The workshop aimed at bridging the gap between the computational engineering community and applied mathematicians and in consequence to unify the scientific language and foster later collaboration. Nonlinear mixed schemes were of particular concern for problems in elasticity and plasticity, but electromagnetics and mathematically related topics were also included.

Mixed finite element methods for elliptic problems are based on a variational description in saddle-point form. Side conditions such as divergence free velocity fields in incompressible fluid dynamics are usually treated in this framework. The appearance of 'soft' side conditions is typical for structural mechanics as is the case with nearly incompressible materials or plates and shells with small thickness parameters. We also mention materials which almost satisfy the Kirchhoff condition, i.e. problems with a high but finite shear stiffness. In such cases, which are by no means 'soft' from the mathematical point of view, mixed methods lead to a more robust discretisation.

The arising stability conditions and computational techniques cannot be understood fully by intuitive mechanical principles; however, from the mathematician's point of view their reasoning is natural, clear and insightful.

Mixed and non-standard finite element methods gain increasing prominence in the prevention of locking phenomena. We highlight a topic which is currently actively investigated: the development of stable and efficient plate and shell elements with regard to shear locking, which is more intricate than volume locking. Here it is important to understand how techniques based on heuristic ideas are consistent with more modern mathematical methods.

Availability of fast solvers is decisive for the competitiveness of numerical techniques. For a variety of applications, multigrid methods are crucial for the efficiency of the implementation.

Methods have been proposed which do not appear plausible if one wants to deduce the algorithms directly from the physical model. The advanced methods depend on rigorous error estimators in order to guarantee that the numerical solutions represent the exact solutions of the physical model.

<div style="text-align: right">

D. Braess
C. Carstensen
K. Hackl

</div>

Workshop: Gemischte und nicht-standard Finite-Elemente-Methoden mit Anwendungen

Table of Contents

Abstracts

A Posteriori Error Estimation for Non-Conforming and Discontinuous Galerkin Finite Element Approximation

Mark Ainsworth

A posteriori error estimation for non-conforming and discontinuous finite element schemes are discussed within a single framework. We show that the same common underlying principles are at work in each case. The ideas are presented in the context of piecewise affine finite element approximation of a second-order elliptic problem for the Crouzeix-Raviart element and symmetric interior penalty discontinuous Galerkin finite element scheme. In both cases, we derive computable upper bounds on the error measured in the broken energy norm along with local lower bounds. Numerical examples are included.

Mixed variational multiscale methods and multiscale finite elements

Todd Arbogast

(joint work with Kirsten J. Boyd)

A longstanding open problem in applied mathematics is to accurately approximate a function that possesses scales smaller than the level of practical discretization. In this work, we consider the approximation on a coarse grid of spacing H of the solution $(\mathbf{u}, p)$ to a second order elliptic problem in mixed form:

$$
\begin{aligned}
\mathbf{u} &= -K\nabla p & &\text{in } \Omega, \\
\nabla \cdot \mathbf{u} &= f & &\text{in } \Omega, \\
\mathbf{u} \cdot \nu &= 0 & &\text{on } \partial\Omega,
\end{aligned}
$$

where $\Omega \subset \mathbf{R}^d$, $d = 2$ or 3, is a bounded domain, K is uniformly elliptic and bounded, and ν is the outward unit normal vector. We assume that K and possibly f exhibit microstructure (i.e., variability or heterogeneity) on a small scale $\epsilon < H$, which induces similar ϵ-scale variation into the solution.

In 1983, Babuška and Osborn [7] gave a practical strategy for problems in one-dimension by defining what they called the *generalized* finite element method, which uses nonpolynomial basis functions. The idea was to solve the differential system locally over the elements (on a mesh that adequately resolves the scale ϵ), and to piece these local solutions together to form the finite element basis functions.

In 1997, Hou and Wu [12, 13] took up this idea and defined *multiscale* finite elements with at least two advances. First, they suggested the use of *oversampling*, i.e., solving the local problems over a larger domain to capture more of the local microstructure. In multiple dimensions, this results in a nonconforming method, because the basis functions do not piece together continuously. A second advance

was to give a multiscale error analysis of the method, illuminating the dependence of the error on both H and ϵ. Later, in 2002, Chen and Hou [11] extended the ideas to mixed finite elements.

Beginning in 1995, Hughes [14, 15] and, independently, Brezzi [8] developed an alternate variational approach, which is called the *variational multiscale* method. The Hilbert space of trial solutions and test functions is divided into two pieces through a direct sum decomposition. The two pieces in some sense represent coarse and fine scales. This decomposition splits both the solution and the variational problem (i.e., the test functions) into coarse and fine scales. If one omits the fine-scale equation and the fine-scale component of the solution, traditional finite element analysis results. However, approximation of the fine-scale components can lead to a better overall approximation, such as greater numerical stability.

Beginning in 1998, Arbogast et al. [6, 1, 2, 3] developed a mixed variant of the variational multiscale method, with the goal of improving the quality of the approximation itself. A coarse grid is used to decompose the solution space $H(\text{Div}) = \bar{\mathbf{V}} \oplus \mathbf{V}'$ and $L^2/\mathbf{R} = \bar{W} \oplus W'$ so as to fulfill two main objectives. First, the decomposition preserves an important physical principle. It conserves mass on both the coarse grid scale and on the fine, or *subgrid*, scales. Secondly, it achieves an important localization property needed for efficient numerical approximation. The subgrid scales from different coarse elements do not interact.

The two-scale variational form can be *upscaled*, meaning that the subgrid parts of the solution can be removed from the equations. If we denote $\mathbf{u} = \bar{\mathbf{u}} + \mathbf{u}' \in \bar{\mathbf{V}} \oplus \mathbf{V}'$ and $p = \bar{p} + p' \in \bar{W} \oplus W'$, then the upscaling operator takes the coarse space $\bar{\mathbf{V}}$ to the fine space $\mathbf{V}' \times W'$, so that $\bar{\mathbf{u}}$ is mapped to $(\mathbf{u}', p')$. This operator is *not* a linear operator; it is *affine*. The linear part is *anti-diffusive* [4]. The constant component of the upscaling operator takes into account the source function f (and external boundary conditions). This is important, since in some problems, such as flow in porous media, f represents wells, which is a small scale feature that must be resolved in the variational framework.

By approximating $(\bar{\mathbf{u}}, \bar{p})$ in the upscaled equation by functions in a standard mixed finite element space, one is lead to a coarse grid mixed finite element method. The standard mixed basis functions are modified by the linear part of the upscaling operator, as in the generalized finite element method. In fact, compared to the usual mixed method on a coarse grid, we obtain a linear system of the same size and sparsity but with a modified matrix and right-hand side vector (since the upscaling operator is affine). Because of these affine terms, this method is not simply a generalized finite element method. However, when the source function has no fine scale component, we obtain exactly the method of Chen and Hou provided that oversampling is not used and we restrict our elements to RT0 [4], the lowest order Raviart-Thomas elements [16]. It is the variational multiscale framework that properly picks up the fine-scale components of f.

Since the construction of the multiscale basis on a fine subgrid parallelizes naturally, the method is very efficient [2]. Numerical examples show that the method

can capture significant fine-scale detail even on very coarse grids. Moreover, it can pick up small-scale effects from wells of diameter much less than H [1, 2, 5].

Multiscale and variational aspects of the method have recently been put on a sound theoretical foundation. The pressure and velocity errors are well approximated. For example, using BDM1, the first order Brezzi-Douglas-Marini spaces [10, 9], on the coarse scale H and RT0 on a fine grid of spacing h to approximate the upscaling operator, the error in $\mathbf{u}$ is $O(H^2)$ and the error in p is $O(h+H^3)$ [3]. The multiscale analysis of Chen an Hou extends to the full variational multiscale method. The main assumptions are that the microstructure of K varies periodically on a scale ϵ, and that the upscaling operator is exact (i.e., not approximated). The error bound for both $\mathbf{u}$ and p is $O(\epsilon + H^m + \sqrt{\epsilon/H})$, where $m = 1$ if RT0 is used and $m = 2$ is BDM1 is used [4].

References

[1] T. Arbogast, *Numerical subgrid upscaling of two-phase flow in porous media*, in Numerical treatment of multiphase flows in porous media, Z. Chen, R. E. Ewing, and Z.-C. Shi, eds., vol. 552 of Lecture Notes in Physics, Springer, Berlin, 2000, pp. 35–49.

[2] T. Arbogast, *Implementation of a locally conservative numerical subgrid upscaling scheme for two-phase Darcy flow*, Comput. Geosci., **6** (2002), pp. 453–481.

[3] T. Arbogast, *Analysis of a two-scale, locally conservative subgrid upscaling for elliptic problems*, SIAM J. Numer. Anal., **42** (2004), pp. 576–598.

[4] T. Arbogast and K. J. Boyd, *Subgrid upscaling and mixed multiscale finite element methods*, in preparation.

[5] T. Arbogast and S. L. Bryant, *A two-scale numerical subgrid technique for waterflood simulations*, SPE J., **7** (Dec. 2002), pp. 446–457.

[6] T. Arbogast, S. E. Minkoff, and P. T. Keenan, *An operator-based approach to upscaling the pressure equation*, in Computational Methods in Water Resources XII, Vol. 1: Computational Methods in Contamination and Remediation of Water Resources, V. N. Burganos et al., eds., Southampton, U.K., 1998, Computational Mechanics Publications, pp. 405–412.

[7] I. Babuška and J. Osborn, *Generalized finite element methods: their performance and their relation to mixed methods*, SIAM J. Numer. Anal., **20** (1983), pp. 510–536.

[8] F. Brezzi, *Interacting with the subgrid world*, in Proceedings of the Conference on Numerical Analysis, Dundee, Scotland, 1999.

[9] F. Brezzi, J. Douglas, Jr., R. Duràn, and M. Fortin, *Mixed finite elements for second order elliptic problems in three variables*, Numer. Math., **51** (1987), pp. 237–250.

[10] F. Brezzi, J. Douglas, Jr., and L. D. Marini, *Two families of mixed elements for second order elliptic problems*, Numer. Math., **47** (1985), pp. 217–235.

[11] Z. Chen and T. Y. Hou, *A mixed multiscale finite element method for elliptic problems with oscillating coefficients*, Math. Comp., **72** (2002), pp. 541–576.

[12] T. Y. Hou and X. H. Wu, *A multiscale finite element method for elliptic problems in composite materials and porous media*, J. Comput. Phys., **134** (1997), pp. 169–189.

[13] T. Y. Hou, X.-H. Wu, and Z. Cai, *Convergence of a multiscale finite element method for elliptic problems with rapidly oscillating coefficients*, Math. Comp., **68** (1999), pp. 913–943.

[14] T. J. R. Hughes, *Multiscale phenomena: Green's functions, the Dirichlet-to-Neumann formulation, subgrid scale models, bubbles and the origins of stabilized methods*, Comput. Methods Appl. Mech. Engrg., **127** (1995), pp. 387–401.

[15] T. J. R. Hughes, G. R. Feijóo, L. Mazzei, and J.-B. Quincy, *The variational multiscale method—a paradigm for computational mechanics*, Comput. Methods Appl. Mech. Engrg., **166** (1998), pp. 3–24.

[16] R. A. Raviart and J. M. Thomas, *A mixed finite element method for 2nd order elliptic problems*, in Mathematical Aspects of Finite Element Methods, I. Galligani and E. Magenes, eds., no. 606 in Lecture Notes in Math., Springer-Verlag, New York, 1977, pp. 292–315.

Enhanced Finite Elements for Discontinuous Solutions in Solids and Structures at Failure

FRANCISCO ARMERO

(joint work with David Ehrlich)

The failure of solids and structures requires the modeling and the numerical resolution of highly non-smooth solutions, involving in the limit solutions with discontinuous displacement fields. Typical examples are not only cracks in brittle materials, but also the large-scale modeling of localized failures like shear bands in metals and soils. The length scale associated to these band can be of the order of microns when typical applications may involve solids and structures of the order of meters or higher. In this context, the presence of bands with highly localized shear strains, for example, can be effectively modeled by surfaces with a discontinuous tangential displacement or slip. Furthermore, local continuum models with strain softening are well-known to lead to serious difficulties due to the lack of a length scale defining the thickness of the localization bands, resulting in ill-posed mathematical problems with physically meaningless solutions since they model the failure of the solid with no dissipation. The need to introduce a localized dissipative mechanism (i.e. dissipating the energy per unit area not volume) appears as a clear need for the correct modeling of these failures. The so-called strong discontinuity approach provides a general framework for the analysis of these discontinuities in the displacements, incorporating a cohesive law in the solid's deformation that allows this objective modeling of the failure of the solid. A main challenge is the need to develop finite element methods approximating the boundary value problem and resolving the discontinuities of the displacements on general, a priori unknown, surfaces.

The approach followed in this work is based on the development of special enhancements of the finite elements that incorporate a discontinuous displacement interpolation at the element level. The local character of the enhancement leads to clear advantages, since it allows the static condensation of the enhanced fields at that level leading to a global problem on the usual nodal displacements only. The discontinuity surface is propagated through a general unstructured meshed, completely unrelated to the discontinuity surface to be modeled. The propagation criterion is based on some physical argument involving the assumed constitutive model in the bulk (e.g. the so-called acoustic tensor condition corresponding mathematically to a change of type of the governing equations). The key aspect that remains is the design of the enhanced strain fields associated to the discontinuous displacement across a given discontinuity surface.

The cases of beams, plates and shells define an especially challenging problem due to the more involved kinematics in these problems when compared to the continuum problem. For example, the strain measures associated to a classical Reissner-Mindlin plate are

$$(1) \qquad \boldsymbol{\kappa} = \nabla^s \boldsymbol{\vartheta} \quad \text{and} \quad \boldsymbol{\gamma} = \nabla w - \boldsymbol{\vartheta} \, ,$$

for the bending and transverse shear strains, respectively, in terms of the deflection w and rotation $\boldsymbol{\vartheta}$ fields. The coupling between the two generalized displacement fields w and $\boldsymbol{\vartheta}$ in the definition of the strain measures (1) is to be noted. The theory developed in this work considers then solutions with discontinuous deflections and rotations along a general surface Γ in the domain $\Omega \subset \mathbb{R}^2$ defining the plate mid-plane. The classical notion of a hinge curve is then recovered.

At the numerical level, a typical finite element Ω_e is divided by a discontinuity segment Γ_e, assumed straight in the proposed formulation. The local interpolated strains $\boldsymbol{\varepsilon}^h = \{\boldsymbol{\kappa}, \boldsymbol{\gamma}\}$ are then written in general form as

$$(2) \qquad \boldsymbol{\varepsilon}^h = \boldsymbol{B}\boldsymbol{d} + \boldsymbol{G}_c \boldsymbol{\xi}_e \qquad \text{in} \quad \Omega_e \backslash \Gamma_e \, ,$$

for the strain operator $\boldsymbol{B}$ (possibly an assumed/mixed strain operator), the nodal displacements $\boldsymbol{d}$ of the base finite element, and a set of local enhanced parameters $\boldsymbol{\xi}_e$ defining a local interpolation of the displacement jumps $[\![w]\!](\boldsymbol{\xi}_e)$ and $[\![\boldsymbol{\vartheta}]\!](\boldsymbol{\xi}_e)$ across Γ_e. As a typical example, we have considered a piece-wise constant interpolation of the rotation jumps $[\![\boldsymbol{\vartheta}]\!]$ together with a linked linear interpolation of the deflection jump $[\![w]\!]$ of the form

$$(3) \qquad \begin{bmatrix} [\![w]\!] \\ [\![\boldsymbol{\vartheta}]\!] \end{bmatrix} = \underbrace{\begin{bmatrix} 1 & \boldsymbol{x} - \boldsymbol{x}_{\Gamma_e} \\ 0 & 1 \end{bmatrix}}_{\boldsymbol{L}_\Gamma} \begin{bmatrix} \xi_{w_e} \\ \boldsymbol{\xi}_{\vartheta_e} \end{bmatrix} \quad \text{for} \quad \boldsymbol{x} \in \Gamma_e \, ,$$

and the articulation point $\boldsymbol{x}_{\Gamma_e} \in \Gamma_e$. The key remaining issue is the definition of the enhanced strain operator $\boldsymbol{G}_c$ defining the influence of the displacement jumps in the strain measures in the bulk of the element $\Omega_e \backslash \Gamma_e$.

The approach considered in this work defines the operator $\boldsymbol{G}_c$ by imposing that the enhanced finite element must be able to model a fully opened hinge, characterized by a zero strain/stress in the bulk of the element $\Omega_e \backslash \Gamma_e$ for any displacement jumps $\boldsymbol{\xi}_e$ (i.e., the zero strains must be in the space of enhanced strains). This strategy avoids the presence of the so-called "stress locking". To this purpose, we identify the nodal displacements associated with this mode as

$$(4) \qquad \boldsymbol{d}_{hinge} := \boldsymbol{d}_{rigid} + \boldsymbol{D}_{hinge} \boldsymbol{\xi}_e \, ,$$

where $\boldsymbol{d}_{rigid}$ refers to a general set of rigid displacements and

$$(5) \qquad \boldsymbol{D}_{hinge}^{(i)} = \begin{cases} \begin{bmatrix} 1 & 0 \\ (\boldsymbol{x}^{(i)} - \boldsymbol{x}_{\Gamma_e}) & 1 \end{bmatrix} & \text{for} \quad i \in \mathcal{J}^+ \, , \\ \boldsymbol{0} & \text{for} \quad i \in \mathcal{J}^- \, . \end{cases}$$

for the nodal coordinates $\boldsymbol{x}^{(i)}$ and the two set of nodes $\mathcal{J}^{\pm}$ of the element on each side of the discontinuity Γ_e. Imposing that the strains (2) vanish for the nodal displacements (4) we arrive at the general formula

$$(6) \qquad \boldsymbol{G}_c = - \sum_{i \in \mathcal{J}^+} \boldsymbol{B}^{(i)} \boldsymbol{D}_{hinge}^{(i)} \ ,$$

for any considered base finite element with $\boldsymbol{B} = [\boldsymbol{B}^{(1)} \boldsymbol{B}^{(2)} \ldots \boldsymbol{B}^{(n_{node})}]$ for the n_{node} nodes of the base finite element. The continuity of the enhanced operator (6) is to be noted. An analysis of (6) can be found in [4] and reference therein.

Considering a linear elastic response for the bulk of the plate characterized by a linear tangent $\mathbb{C}$, the final set of finite element equations reads

$$(7) \qquad \boldsymbol{R} := \boldsymbol{f}_{ext} - \int_{\Omega} \boldsymbol{B}^T \mathbb{C} \left[\boldsymbol{B}\boldsymbol{d} + \boldsymbol{G}_c \boldsymbol{\xi}_e \right] \ d\Omega = 0 \ ,$$

$$(8) \qquad \boldsymbol{r}_e := - \int_{\Omega_e} \boldsymbol{G}_e^T \mathbb{C} \left[\boldsymbol{B}\boldsymbol{d} + \boldsymbol{G}_c \boldsymbol{\xi}_e \right] \ d\Omega - \int_{\Gamma_e} \boldsymbol{L}_\Gamma^T \boldsymbol{T}(\boldsymbol{\xi}_e) \ d\Gamma = 0 \ ,$$

with the standard global equation (7) corresponding to the equilibrium of the plate and the local equation (8) in terms of "equilibrium" operators $\boldsymbol{G}_e$. Equation $(8)_2$ imposes that the driving tractions $\boldsymbol{T}$ along the hinge, defined in terms of the displacement jumps $\boldsymbol{\xi}_e$ by the localized cohesive law, are given in terms of the stresses in the bulk. The operator $\boldsymbol{G}_e$ can be constructed as a piece-wise polynomial such that this local equilibrium relation is enforced exactly for the assumed interpolations of the stress field in the base finite element (see [4]).

The local character of equation (8) allows the elimination of the enhanced parameters $\boldsymbol{\xi}_e$ modeling the displacement jumps at the element level. The final system of equations involves only the nodal displacements $\boldsymbol{d}$. This in combination with the fact that the above developments can be combined with any base element, through the strain operator $\boldsymbol{B}$, makes the proposed approach especially interesting. We have considered triangular and quadrilateral finite elements, in the basic displacement form, mixed and assumed strain elements (like the MITC-4 assumed strain quad for the plate problem discussed in this brief summary).

We refer to [1, 2] and [3] for complete details in the context of beams and frames, and [4] for the formulation of finite elements for the modeling of localized failures of plates. See also the references therein for application to other problems in the continuum, both in the infinitesimal and finite deformation ranges, including coupled thermomechanical and poroplastic problems.

References

[1] F. Armero and D. Ehrlich, *An Analysis of Strain Localization and Wave Propagation in Plastic Beams at Failure*, Computer Methods in Applied Mechanics and Engineering, (2004), 193, 3129-3171.

[2] D. Ehrlich and F. Armero, *Finite Elements for the Analysis of Plastic Hinges in Beams and Frames*, Computational Mechanics, (2005), 35, 237-264.

[3] F. Armero and D. Ehrlich, *Numerical Modeling of Softening Hinges in Thin Euler-Bernoulli Beams*, (2004), submitted.

[4] F. Armero and D. Ehrlich, *Finite Element Methods for the Multi-Scale Modeling of Softening Hinge Lines in Plates at Failure*, Computer Methods in Applied Mechanics and Engineering, (2004), in press.

Advantage and Disadvantage of the Method of Enhanced Assumed Strains

Dietrich Braess

(joint work with Carsten Carstensen and Daya Reddy)

Abstract. Finite elements with enhanced assumed strains are equivalent to mixed methods associated to the Hellinger–Reissner principle. The softening of the energy which avoids locking phenomena and the role of the hidden LBB condition are elucidated for nearly incompressible material.

1. The Need of Softening

In structural mechanics often *problems with a small parameter* are encountered which give rise to locking phenomena:
- nearly incompressible material (volume locking),
- plates, beams and cantilevers (shear locking),
- shells (membrane locking),
- 3-dim. models of plates and shells (thickness locking).

Locking means that a portion of the stored energy is too stiff and must be softened. Here appropriate variational formulations and finite elements are required which are able to cope with these situations. In particular, the stiff part of the energy has to be softened.

If we exclude shells, the energy that is to be minimized is of the following form

$$\Pi(u) = \frac{1}{2}a_0(u, u) + \frac{1}{2t^2}\int_\Omega (Bu)^2 dx - (f, u).$$

Here a_0 is a (nice) quadratic form that can be treated by standard methods, t is the small parameter, B a mapping into $L_2(\Omega)$, and the last term represents the external load.

We consider a nearly incompressible material, then $a_0(u, u) = \mu \int \varepsilon(u)^2 dx$, $t^2 = \frac{\mu}{\lambda}$ and

$$Bu = \operatorname{div} u.$$

The kernel of the operator, $\ker u = \{v \in H_0^1(\Omega); \operatorname{div} v = 0 \ a.e.\}$, is a very rich (thick) space. – This is quite different in the finite element space, in particular when the quadrilateral Q_1 element (with bilinear functions) is chosen. The kernel consists of the rigid body motions and a linear one direction shear only. The kernel is a low dimensional space, and the dimension is not increased by refinements of the finite element mesh.

[Similarly, when the Mindlin plate is considered, we have $u = (\theta, w)$ with θ being the rotation, w the vertical displacement and

$$Bu := \theta - \nabla w$$

is the shear term that has to be softened.]

The canonical way of softening via a mixed method with penalty [2, p. 301] is not popular.

2. Softening Behavior of the Hellinger–Reissner Formulation

Another way of softening is the use of finite elements with enhanced assumed strains [4]. It is equivalent to the mixed method associated to the Hellinger–Reissner principle. For convenience, we describe it for the mixed formulation of the Poisson equation $\sigma - \nabla u = 0$, $\operatorname{div} \sigma = -f$, since the analogous treatment of the Lamé equations is less transparent. Here we consider the pairing with the spaces $L_2(\Omega)$-$H^1(\Omega)$ and not $H(\operatorname{div}, \Omega)$-$L_2(\Omega)$. Let $S_h \subset L_2(\Omega)$ and $V_h \subset H^1(\Omega)$ be the finite element spaces for σ and u, resp. Then

$$
(1) \qquad
\begin{aligned}
(\sigma_h, \tau) - (\tau, \nabla u_h) &= 0 && \forall \tau \in S_h, \\
-(\sigma_h, \nabla v) &= -(f, v) && \forall v \in V_h.
\end{aligned}
$$

Let P_{S_h} be the L_2-orthogonal projector onto S_h. The first equation says $\sigma_h = P_{S_h}(\nabla u_h)$, and the second equation that we are computing the solution of the minimum problem

$$\frac{1}{2} \int_\Omega (P_{S_h} \nabla u_h)^2 \, dx - \int_\Omega f u_h dx \to \min!$$

Since the projection reduces the energy, we have got a softening effect.

Instead of defining the target space S_h of the projection, we can specify the orthogonal complement. Note that $\sigma_h = P_{S_h}(\nabla u_h)$ implies (in the framework of the Lamé equation the elasticity matrix is found as a factor)

$$\sigma_h = \nabla u_h + \tilde{\varepsilon}_h \quad \text{with } \tilde{\varepsilon}_h \in \tilde{E}_h \perp S_h.$$

Here $\tilde{E}_h$ is the space of enhanced strains.

Lemma 1. [5] *The mixed method (1) is equivalent to the variational formulation*

$$
(2) \qquad
\begin{aligned}
(\nabla u_h, \nabla v)_{0,\Omega} &+ (\tilde{\varepsilon}_h, \nabla v)_{0,\Omega} &= (f, v)_{0,\Omega} && \in V_h, \\
(\nabla u_h, \tilde{\eta})_{0,\Omega} &+ (\tilde{\varepsilon}_h, \eta)_{0,\Omega} &= 0 && for \eta \in \tilde{E}_h,
\end{aligned}
$$

if the space $\tilde{E}_h$ of enhanced gradients satisfies the decomposition rule $\nabla V_h \subset S_h \oplus \tilde{E}_h$.

Now it is clear that one cannot combine arbitrary pairs of spaces V_h and $\tilde{E}_h$ since one has to guarantee the LBB condition. This is often forgotten. Fortunately it can be expressed in terms of displacements and enhanced strains.
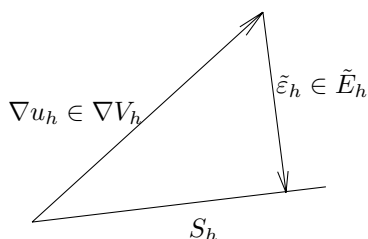
FIGURE 1. Projection of ∇u_h to S_h and $\tilde{E}_h$ in the EAS method.

Lemma 2. [2, p.153] *The spaces V_h and S_h satisfy the inf-sup condition with a constant $\beta > 0$ if and only if a strengthened Cauchy inequality holds,*

$$(\nabla v_h, \eta_h)_{0,\Omega} \le \sqrt{1 - \beta^2} \|\nabla v_h\|_0 \|\eta_h\|_0 \quad \text{for } v_h \in V_h, \eta_h \in \tilde{E}_h.$$

3. INTERPOLATION

In particular, volume locking disappears if the divergence is replaced by its mean value on each element. The volume term reads

$$(3) \qquad \frac{\lambda}{2} \sum_{T \subset \Omega} \int_T (\overline{\text{div}}\, v_h)^2 dx$$

This projection is also achieved with enhanced strains by Simo and Rifai [4]. The projection is related to the Stokes problem and the Q_1-P_0 element. Unfortunately the Q_1-P_0 element is unstable. This induces complications also in 7 (or more) almost equivalent remedies of locking known in engineering literature. Fortunately, a stable variant is obtained by a filter, and the filtered element is sufficient for the EAS method and linear problems for the following reason.

The efficient divergence of a finite element pair $(v_h, \tilde{\varepsilon}_h)$ is obviously $\text{div}\, v_h + \text{trace}\, \tilde{\varepsilon}_h$. There will be no locking if we find an interpolation operator $I_h : v \mapsto (v_h, \tilde{\varepsilon}_h)$ with the usual approximation properties and the additional prperty

$$(4) \qquad \text{div}\, v_h + \text{trace}\, \tilde{\varepsilon}_h = 0 \quad \text{if } \text{div}\, v = 0.$$

An interpolation with these properties is indeed given by the Stokes problem with the filtered Q_1-P_0 element [3] and related to (3). Thus the EAS method provides a stable locking-free element without the need of implementing the filter. In particular, the regularity result in [1] admits a robust approximation with a constant that is independent of the large parameter λ [3],

$$\lambda \|\, \text{div}\, u - \text{div}\, u_h - \text{trace}\, \tilde{\varepsilon}_h\|_0 + \|u - u_h\|_1 \le c\, h \|f\|_0.$$

Finally, we emphasize that the pairs of spaces must be well balanced. *If the space $\tilde{E}_h$ is too small, then we do not achieve property (4). If the space $\tilde{E}_h$ is too large, then stability is lost.*

References

[1] Douglas N. Arnold, and L. Ridgway Scott and Michael Vogelius. Regular inversion of the divergence operator with Dirichlet boundary conditions on a polygon. Ann. Scuola Norm. Sup. Pisa Cl. Sci. Seris IV, 15, 2, 169–192 (1988).

[2] Dietrich Braess. *Finite Elements.* Cambridge University Press, Cambridge, (2001).

[3] D. Braess, C. Carstensen and B.D. Reddy, Uniform convergence and a posteriori error estimators for the enhanced strain finite element method. Numer. Math. 96, 461–479 (2004)

[4] J.C. Simo and Rifai, M. S. (1990). A class of mixed assumed strain methods and the method of incompatible modes. Internat. J. Numer. Methods Engrg., **29**, 8, 1595–1638.

[5] Seung T. Yeo and Byung C. Lee. Equivalence between enhanced assumed strain method and assumed stress hybrid method based on the Hellinger-Reissner principle. Internat. J. Numer. Methods Engrg., 39, 18, 3083–3099 (1996).

The inf-sup condition for the Stokes equations: A constructive approach in general domains

RICARDO G. DURÁN

(joint work with G. Acosta, M. A. Muschietti)

A fundamental result for the theoretical and numerical analysis of the Stokes equations in a bounded domain $\Omega \subset \mathbb{R}^n$ is the so called *inf-sup* condition. An equivalent way of stating this condition is to say that, for any $f \in L^2(\Omega)$ with vanishing mean value in Ω, there exists $\mathbf{u} \in H_0^1(\Omega)^n$ such that

$$(1) \qquad\qquad \operatorname{div} \mathbf{u} = f \quad \text{in} \ \ \Omega$$

and

$$(2) \qquad\qquad \|\mathbf{u}\|_{H^1(\Omega)^n} \leq C\|f\|_{L^2(\Omega)},$$

where C is a constant which depends only on the domain Ω.

Several arguments have been given to prove this result. For example, if the domain has a smooth boundary or if it is a convex polygon, the existence of $\mathbf{u}$ can be proved by using a priori estimates for elliptic equations (see for example [5]).

Another possibility is to construct explicit solutions of (1). There are several motivations to use a constructive approach. First, it provides some information about the dependence of the constant C on the geometry of the domain Ω. On the other hand, the explicit construction can be used to obtain an estimate like (2) in different norms. For example, in [7], estimates in weighted norms were obtained (these weighted norms can be used to obtain error estimates in the L^∞-norm for finite element approximations of the Stokes equations (see [8])).

In this lecture we show how explicit solutions of (1) can be obtained for a very wide class of domains.

In order to present the ideas we recall first the construction for domains Ω which are star-shaped with respect to a ball B (see [3, 7]).

Given a smooth function ϕ let us call $\overline{\phi} = \int_\Omega \phi\omega$, where ω is an arbitrary smooth function such that $\int_\Omega \omega = 1$ and $\operatorname{supp}\omega \subset B$. A key point in our construction is

to recover $\phi - \overline{\phi}$ from its gradient. To simplify notation we assume that the center of the ball B is at the origin.

If for any $y \in \Omega$ and $s \in [0,1]$ we call $\gamma(s,y) = (1-s)y$ then, for any $z \in B$, the segment joining y with z is parametrized by $\gamma(s,y)+sz$. Therefore, integrating over the segments $[y,z]$, we have $\phi(y) - \phi(z) = -\int_0^1 (\dot{\gamma}(s,y) + z) \cdot \nabla\phi(\gamma(s,y) + sz)ds$, where $\dot{\gamma}(s,y)$ indicates the derivative with respect to s. Multiplying by $\omega(z)$, integrating on z and making the change of variable $x = \gamma(s,y) + sz$, we obtain the representation

$$(3) \qquad (\phi - \overline{\phi})(y) = -\int_\Omega G(x,y) \cdot \nabla\phi(x)\,dx,$$

where $G = (G_1, \cdots, G_n)$ is defined as

$$G(x,y) = \int_0^1 \frac{(x-y)}{s} \omega\left(\frac{x - \gamma(s,y)}{s}\right) \frac{1}{s^n}\,ds.$$

If for $f \in L^1(\Omega)$ such that $\int_\Omega f = 0$ we define

$$(4) \qquad \mathbf{u}(x) = \int_\Omega G(x,y)\,f(y)\,dy,$$

it follows from (3) that $\int_\Omega f(y)\phi(y)\,dy = -\int_\Omega \mathbf{u}(x) \cdot \nabla\phi(x)\,dx$, for any $\phi \in C_0^\infty(\Omega)$, and therefore $\mathbf{u}$ is a solution of (1). On the other hand, using that $\operatorname{supp}\omega \subset B$, it is not difficult to see that $G(x,y) = 0$ for every $x \in \partial\Omega$, and consequently $\mathbf{u}$ vanishes on $\partial\Omega$.

Now, our goal is to extend this construction for more general domains. It is known that the domain can not be arbitrary. Indeed, several counterexamples have been given to show that solutions of (1) satisfying (2) may not exist if the domain has external cusps. We give here an elementary counterexample due to G. Acosta.

First we recall that, using functional analysis arguments, it can be shown that the *inf-sup* condition implies the following result known as "Lions lemma":

$$f \in L^2(\Omega) \iff f \in H^{-1}(\Omega) \quad \text{and} \quad \nabla f \in H^{-1}(\Omega)^n.$$

(and the results are equivalent for domains for which the compact imbedding of $H^1(\Omega)$ into $L^2(\Omega)$ holds).

Let $\Omega := \{(x,y) \in \mathbb{R}^2 : 0 < x < 1, 0 < y < x^2\}$ and $f(x,y) = x^{-2}$. An elementary computation shows that $f \notin L^2(\Omega)$. However, $f \in H^{-1}(\Omega)$ and $\nabla f \in H^{-1}(\Omega)^2$. Indeed, $\frac{\partial f}{\partial x} = \frac{\partial(-2yx^{-3})}{\partial y}$, and it is easy to see that $-2yx^{-3} \in L^2(\Omega)$ and therefore $\frac{\partial f}{\partial x} \in H^{-1}(\Omega)$. In a similar way we can see that $f \in H^{-1}(\Omega)$. Analogous counterexamples can be constructed for the more general domain $\Omega := \{(x,y) \in \mathbb{R}^2 : 0 < x < 1, 0 < y < x^\alpha\}$, for any $\alpha > 1$ [1].

In view of these counterexamples, we have to work with a class of domains which exclude domains with external cusps. Consequently, it seems natural to consider the John domains which is a very general class containing in particular the Lipschitz domains (a John domain can have a "very bad" boundary but it can not have external cusps). A bounded open set $\Omega \subset R^n$ is a John domain if, for

a fixed $x_0 \in \Omega$, there exists a function $\gamma : [0,1] \times \Omega \to \Omega$ and constants K and δ such that,

    1) $\gamma(0,y) = y$, $\gamma(1,y) = x_0$
    2) $d(\gamma(s,y)) \geq \delta s$
    3) $|\dot{\gamma}(s,y)| \leq K$,

where $d(x)$ denotes the distance of x to the boundary of Ω. Given a John domain there are many ways to choose the curves joining x_0 with y. We have to choose the curves in such a way that other properties needed in the proofs are satisfied (see [2]).

Using the curves given by $\gamma(s,y)$ we can repeat the construction given for the star-shaped domains. Assume that $x_0 = 0$ and take the averaging function ω such that $\operatorname{supp} \omega \subset B(0, \delta/2)$. Integrating over the curves $\gamma(s,y) + sz$ joining $z \in B(0, \delta/2)$ with $y \in \Omega$ we obtain the representation (3) where now

$$(5) \qquad G(x,y) := \int_0^1 \left\{ \dot{\gamma}(s,y) + \frac{x - \gamma(s,y)}{s} \right\} \omega\left(\frac{x - \gamma(s,y)}{s} \right) \frac{1}{s^n} \, ds.$$

As a consequence a solution of (1) is obtained as in (4) (that $\mathbf{u}$ vanishes on the boundary follows now from the fact that $\operatorname{supp} \omega \subset B(0, \delta/2)$ and using that $d(\gamma(s,y)) \geq \delta s$).

Up to this point our construction made use only of elementary results. The more difficult point is to prove that $\mathbf{u}$ satisfies (2). In order to obtain this result we make use of the theory of singular integral operators of Calderón and Zygmund [6] (see [2] for details). We also obtain the generalization to the L^p case, $1 < p < \infty$, of the estimate (2). The results are summarized in the following theorem.

Theorem: Let $\Omega \subset \mathbb{R}^n$ be a bounded John domain. Given $f \in L^p(\Omega)$, $1 < p < \infty$, such that $\int_\Omega f = 0$, let $\mathbf{u}$ be the function given by (4) with G defined as in (5). Then, $\mathbf{u} \in W_0^{1,p}(\Omega)$ and satisfies (1) and the estimate

$$(6) \qquad\qquad\qquad \|\mathbf{u}\|_{W^{1,p}(\Omega)^n} \leq C \|f\|_{L^p(\Omega)}$$

with a constant C depending only K, δ, p, ω and n.

An interesting question is whether the class of John domains is the more general one for which a solution of (1) vanishing on the boundary and satisfying (6) can be proved. A partial result in this direction is given in the following theorem which can be obtained from the previous theorem and the results given in [4].

Theorem: Let $\Omega \subset \mathbb{R}^2$ be a simply connected domain. Then, Ω is a John domain if and only if, for every $1 < p < \infty$, a solution $\mathbf{u} \in W^{1,p}(\Omega)^n$ of (1) satisfying (6) exists for any $f \in L^p(\Omega)$ with vanishing mean value.

References

[1] G. Acosta, personal communication.
[2] G. Acosta, R. G. Durán, M. A. Muschietti, *Solutions of the divergence operator on John domains*, preprint, http://mate.dm.uba.ar/ rduran/papers.html
[3] M. E. Bogovskii, *Solution of the first boundary value problem for the equation of continuity of an incompressible medium*, Soviet Math. Dokl. **20** (1979), 1094–1098.
[4] S. Buckley, P. Koskela, *Sobolev-Poincaré implies John*, Math. Ress. Lett. **2** (1995), 577–593.

[5] S. C. Brenner and L. R. Scott, *The Mathematical Theory of Finite Element Methods*, Springer-Verlag, Berlin, 1994.

[6] A. P. Calderón, A. Zygmund, *On singular integrals*, Amer. J. Math. **78** (1956), 289–309.

[7] R. G. Durán, M. A. Muschietti, *An explicit right inverse of the divergence operator which is continuous in weighted norms*, Studia Math. **148** (2001), 207–219.

[8] R. G. Durán, R. H. Nochetto, *Weighted inf-sup condition and pointwise error estimates for the Stokes problem*, Math. Comp. **54** (1990), 63–79.

Continuous/Discontinuous Galerkin methods for fourth-order partial differential equations

Krishna Garikipati

(joint work with G. Engel, L. Mazzei, L. Molari, T. J. R. Hughes, M. G. Larsson, R. L. Taylor, F. Ubertini, G. N. Wells)

Fourth-order partial differential equations arise in the strong forms of the Euler-Bernoulli Thin Beam Theory and Poisson-Kirchhoff Plate Theory in structural mechanics, Strain Gradient Theories in continuum mechanics, and Diffuse Interface Theory (the Cahn-Hilliard Equation) in materials physics. The Galerkin finite element method for these problems involves second-order spatial derivatives on the solution and its weighting function in the weak form. The requirement of higher-order continuity on the solution has led to the use of C^1-continuous functions for the beam and plate equations, mixed methods for the plate and strain gradient equations, and reformulation into a coupled second-order system of equations for the diffuse interface theory. The use of C^1 functions is beyond the realm of practicability, while mixed methods for strain gradient theories have not proved robust or computationally-efficient yet. A class of continuous/discontinuous Galerkin (C/DG) methods has been developed to address all of these difficulties while maintaining robustness and numerical efficiency. In this communication we briefly summarize some of these higher-order equations, the C/DG methods developed, and error analyses.

1. Strain gradient damage in one dimension

The strain gradient damage model has been discussed in detail in [1]. Here we provide a summary: The governing equations are

$$\sigma = [1 - D(\kappa)]\mathbb{E}\colon \varepsilon, \qquad \text{Stress-strain relation}$$

$$0 \leq D(\kappa) \leq 1, \qquad \text{Damage variable}$$

$$\frac{\partial \kappa}{\partial t} \geq 0,\ \overline{\varepsilon} - \kappa \leq 0,\ \frac{\partial \kappa}{\partial t}(\overline{\varepsilon} - \kappa) = 0, \quad \text{Kuhn-Tucker relations}$$

$$(1) \qquad \overline{\varepsilon} := \varepsilon_{\text{eq}} + c^2 \nabla^2 \varepsilon_{\text{eq}}, \qquad \text{Strain gradient dependence.}$$

The stress "softens" with strain during the growth of damage. The strain gradient damage model is motivated by the mesh-dependent pathology obtained

in standard (local) inelastic models with softening in the stress-strain response, and c is an material length scale.

Peerlings and co-workers [1] discuss a reformulation of this mathematical model to avoid the difficulty of representing the strain gradient terms. Observe that, on substituting the Kuhn-Tucker relation into the stress-strain relation, (1) becomes a fourth-order partial differential equation in regions of increasing damage. Our C/DG mixed formulation of this problem appeared in [2]. A simplified, one-dimensional version of this formulation is written with $\varepsilon_{eq} = \varepsilon$:

Find $u^h \in \mathscr{S}^h = \{u^h \in H^1(\Omega)|u^h = g$ on $\Gamma_u\}$ and $\overline{\varepsilon}^h \in \mathscr{E}^h \subset L^2(\Omega)$, s. t. $\forall\, w^h \in \mathscr{V}^h = \{w^h \in H^1(\Omega)|w^h = 0$ on $\Gamma_u\}$ and $\nu^h \in \mathscr{E}^h$

$$(2) \qquad \int_\Omega (w^h_{,x}\,(1 - D(\kappa))\,E u^h_{,x})\mathrm{d}x - w^h t|_{\Gamma_\sigma} = 0,$$

$$\int_{\widetilde{\Omega}} \left(\nu^h(\overline{\varepsilon}^h - \varepsilon^h) + \nu^h_{,x} c^2 \varepsilon^h_{,x}\right) \mathrm{d}x - (\llbracket \nu^h \rrbracket c^2 \langle \varepsilon^h_{,x}\rangle + \langle \nu^h_{,x}\rangle c^2 \llbracket \varepsilon^h \rrbracket)|_{\widetilde{\Gamma}}$$

$$(3) \qquad\qquad\qquad +\alpha \frac{c^2}{h}\llbracket \nu^h \rrbracket \llbracket \varepsilon^h \rrbracket|_{\widetilde{\Gamma}} = 0$$

In (3) the jump and average operators, $\llbracket \bullet \rrbracket$ and $\langle \bullet \rangle$ respectively, are defined in the usual manner on the union of inter-element boundaries, $\widetilde{\Gamma}$, and $\widetilde{\Omega}$ is the union of element interiors. The parameter, α, which multiplies the interior-penalty term, is dimensionless. The Young's modulus is E. Consistency of this method was shown in [2].

An error analysis of (3) was carried out in [3]. Detailed numerical examples, and a comparison of numerical results with convergence rates also established in the same paper are also included therein.

2. Strain gradient elasticity in one dimension

The strain gradient elasticity theory used here is a linearized, one-dimensional version of Toupin's formulation [4]. It serves as a model for certain theories of strain gradient plasticity. For a shear layer, letting the displacement be denoted by u, the governing equations are:

$$(\mu u_{,x})_{,x} - (\mu c^2 u_{,xx})_{,xx} + f = 0 \quad \text{in } \Omega$$
$$u = g \quad \text{on } \Gamma_g$$
$$u_{,x} \cdot n = q \quad \text{on } \Gamma_q$$
$$\mu c^2 u_{,xx} = r \quad \text{on } \Gamma_r$$
$$(4) \qquad \mu u_{,x} \cdot n - (\mu c^2 u_{,xx})_{,x} \cdot n = t \quad \text{on } \Gamma_t,$$

where the boundary conditions in $(4)_2$–$(4)_5$ are for the displacement, strain, couple stress traction, and the traction, respectively. The shear modulus is μ, and c is the material length scale as in Section 1. The fourth-order term is seen explicitly in $(4)_1$. The C/DG single-field weak form is:

Find $u^h \in \mathscr{S}^h$ such that $B_{\mathrm{s}}\left(w^h, u^h\right) = L_{\mathrm{s}}\left(w^h\right) \quad \forall w^h \in \mathscr{V}^h$, where

$$B_{\mathrm{s}}\left(w^h, u^h\right) = \int\limits_{\widetilde{\Omega}} \left(w^h_{,x}\mu u^h_{,x} + w^h_{,xx}\mu c^2 u^h_{,xx}\right)\, dx - [\![w^h_{,x}]\!]\langle\mu c^2 u^h_{,xx}\rangle_{\widetilde{\Gamma}}$$

$$- \langle\mu\rangle c^2 w^h_{,xx}[\![u^h_{,x}]\!]_{\widetilde{\Gamma}} + \tau\, [\![w]\!]^h_{,x}[\![u^h_{,x}]\!]_{\widetilde{\Gamma}} - w^h_{,x}\cdot n\,\mu c^2 u^h_{,xx}\big|_{\Gamma_q}$$

(5)
$$- \mu c^2 w^h_{,xx}\, u^h_{,x}\cdot n\big|_{\Gamma_q} + \tau_q\, w^h_{,x}\cdot n\, u^h_{,x}\cdot n\big|_{\Gamma_q}$$

$$L_{\mathrm{s}}\left(w^h\right) = \int\limits_{\widetilde{\Omega}} w^h\, f\, dx + w^h_{,x}\cdot n\, r\big|_{\Gamma_r} - \mu c^2 w^h_{,xx}\, q\big|_{\Gamma_q} + w^h\, t\big|_{\Gamma_t}$$

(6)
$$+ \tau_q\, w^h_{,x}\cdot n\, q\big|_{\Gamma_q},$$

The stabilization parameters are $\tau = \mathcal{O}\left(\frac{\mu c^2}{h}\right)$, and $\tau_q = \mathcal{O}\left(\frac{\mu c^2}{h}\right)$. For this method we have established convergence rates in the energy and L^2 norms, respectively:

$$(7) \quad |\!|\!|e|\!|\!|^2 \leq C\sum_{e=1}^{\mathrm{nel}} h_e^{2(k-1)}\,|u|^2_{H^{k+1}(\Omega_e)}; \quad \|e\|^2 \leq C\sum_{e=1}^{\mathrm{nel}} h_e^{2(k+1)}\,|u|^2_{H^{k+1}(\Omega_e)}.$$

Numerical results compared with these rates of convergence are summarized in [5]. Also included are details of the formulation for strain gradient elasticity, for Euler-Bernoulli Beam Theory and Poisson-Kirchhoff Plate Theory.

3. Summary

The C/DG method outlined in Section 2 is being extended to the Cahn-Hilliard equation, a fourth-order diffusion equation that describes diffuse interfaces that develop during phase separation of binary alloys.

References

[1] R.H.J. Peerlings, R. de Borst, A.M. Brekelmans, J.H.P. de Vree, *Gradient enhanced damage for quasi-brittle materials*, International Journal for Numerical Methods in Engineering **39** (1996), 3391–3403.

[2] G.N. Wells, K. Garikipati, L. Molari, *A discontinuous Galerkin formulation for a strain gradient-dependent continuum model*, Computer Methods in Applied Mechanics and Engineering **193** (33-35) (2004), 3633–3645.

[3] G.N. Wells, L. Molari, K. Garikipati, F. Ubertini, *A discontinuous Galerkin method for strain gradient-dependent damage: Study of interpolations and convergence*, Computer Methods in Applied Mechanics and Engineering, to appear, (2005).

[4] R.A. Toupin, *Elastic materials with couple-stresses*, Archive for Rational Mechanics and Analysis, **11** (1962), 385–414.

[5] G. Engel, K. Garikipati, T.J.R. Hughes, M.G. Larson, L. Mazzei, R.L. Taylor, *Continuous/discontinuous finite element approximations of fourth-order elliptic problems in structural and continuum mechanics with applications to thin beams and plates, and strain gradient elasticity*, Computer Methods in Applied Mechanics and Engineering **191** (34) (2002), 3669–3750.

Nitsche's method for interface problems
Peter Hansbo

Consider the typical Poisson model problem of finding u such that

(1) $$-\Delta u = f \text{ in } \Omega, \quad u = 0 \text{ on } partial\Omega,$$

where Ω is a bounded domain in two or three space dimensions, with boundary $\partial\Omega$ and with f a given function.

For domain decomposition purposes it is beneficial to rephrase (1) as follows. Consider an (artificial) interface Γ dividing Ω into two open sets Ω_1 and Ω_2, with interface $\Gamma = \overline{\Omega}_1 \cap \overline{\Omega}_2$. For any sufficiently regular function u in $\Omega_1 \cup \Omega_2$ we define the jump of u on Γ by $[\![u]\!] := u_1|_\Gamma - u_2|_\Gamma$, where $u_i = u|_{\Omega_i}$ is the restriction of u to Ω_i. Conversely, for u_i defined in Ω_i we identify the pair (u_1, u_2) with the function u which equals u_i on Ω_i. For definiteness, we define $\boldsymbol{n}$ as the outward pointing unit normal to Ω_1, and we define $\partial_n := \boldsymbol{n} \cdot \nabla$. We can then formulate the following variant of Poisson's equation:

(2)
$$\begin{aligned}
-\Delta u &= f &&\text{in} & \Omega_1 \cup \Omega_2, \\
u &= 0 &&\text{on} & \partial\Omega, \\
[\![u]\!] &= 0 &&\text{on} & \Gamma, \\
[\![\partial_n u]\!] &= 0 &&\text{on} & \Gamma.
\end{aligned}$$

Invoking the smoothness assumption $u \in H^2(\Omega)$, we have that (2) is equivalent to (1) with $u|_{\Omega_i} = u_i, \quad i = 1, 2$. We may then write $u = (u_1, u_2) \in V_1 \times V_2$ with the continuous spaces

$$V_i = \left\{ v_i \in H^1(\Omega_i) : \ \partial v_i / \partial n_i \in L_2(\Gamma), \ v_i|_{\partial\Omega \cap \partial\Omega_i} = 0 \right\}, \quad i = 1, 2.$$

To formulate the method, we suppose that we have finite element partitionings $\mathfrak{T}_h^i$ of the subdomains Ω_i. We assume that at least one of the meshes contains shape regular elements bordering to the interface. For definiteness, we define this to be $\mathfrak{T}_h^1$.

We seek the approximation $U = (U_1, U_2)$ in the space $V^h = V_1^h \times V_2^h$, where

$$V_i^h = \left\{ v_i \in V_i : \ v_i|_K \text{ is a polynomial of degree } p \text{ for all } K \in \mathfrak{T}_h^i \right\}.$$

Nitsche's method for the problem (2) can then be written as follows (cf. [1]): find $U \in V^h$ such that

(3) $$a_h(U, v) = L(v) \quad \forall v \in V^h,$$

with

(4) $$\begin{aligned}
a_h(w, v) \ &:= \ \sum_{i=1}^{2} (\nabla w_i, \nabla v_i)_{\Omega_i} + \gamma(h^{-1}\,[\![w]\!], [\![v]\!])_\Gamma \\
&\quad - (\partial_n w_1, [\![v]\!])_\Gamma - (\partial_n v_1, [\![w]\!])_\Gamma
\end{aligned}$$

and

(5) $$L(v) := \sum_{i=1}^{2} (f, v_i)_{\Omega_i}.$$

This is a consistent method: multiplying the first equation in (2) with v_i, integrating over Ω_i, using Greens formula and the fact that $\partial_n u_1 = \partial_n u_2$ on Γ yields

$$
\begin{aligned}
L(v) &= \sum_{i=1}^{2} (f, v_i)_{\Omega_i} = \sum_{i=1}^{2} (\nabla u_i, \nabla v_i)_{\Omega_i} - (\partial_n u_1, v_1)_\Gamma + (\partial_n u_2, v_2)_\Gamma \\
(6) \qquad &= \sum_{i=1}^{2} (\nabla u_i, \nabla v_i)_{\Omega_i} - (\partial_n u_1, [\![v]\!])_\Gamma.
\end{aligned}
$$

Since $[\![u]\!] = 0$ on Γ we have

$$
(7) \qquad\qquad 0 = -(\partial_n v_1, [\![u]\!])_\Gamma + \gamma(h^{-1} [\![u]\!], [\![v]\!])_\Gamma.
$$

Finally, adding (6) and (7) shows consistency in that the solution $u = (u_1, u_2)$ to (2) satisfies

$$
(8) \qquad\qquad a_h(u, v) = L(v) \quad \forall v \in V^h.
$$

As for the stability, we have that

$$
a_h(U, U) = \sum_i (\nabla U_i, \nabla U_i)_{\Omega_i} - 2(\partial_n U_1, [\![U]\!])_\Gamma + (\gamma h^{-1} [\![U]\!], [\![U]\!])_\Gamma
$$

i.e.,

$$
a_h(U, U) \geq \|\nabla U_i\|_{L_2(\Omega_i)}^2 - 2\|\partial_n U_1\|_{L_2(\Gamma)} \| [\![U]\!] \|_{L_2(\Gamma)} + \frac{\gamma}{h} \| [\![U]\!] \|_{L_2(\partial\Omega)}^2
$$

i.e., using that $(ax - y/a)^2 \geq 0$ implies $a^2 x^2 + y^2/a^2 \geq 2xy$,

$$
a_h(U, U) \geq \sum_i \|\nabla U_i\|_{L_2(\Omega_i)}^2 - \frac{h}{\epsilon}\|\partial_n U_1\|_{L_2(\Gamma)}^2 - \frac{\epsilon}{h}\| [\![U]\!] \|_{L_2(\Gamma)}^2 + \frac{\gamma}{h}\| [\![U]\!] \|_{L_2(\Gamma)}^2.
$$

Invoking now the inverse inequality

$$
(9) \qquad\qquad \|h\,\partial_n U_1\|_{L_2(\Gamma)}^2 \leq C_I \|\nabla U_1\|_{L_2(\Omega_1)}^2,
$$

valid for discrete U_1, we find that $a_h(U, U)$ is positive if we choose $\gamma > \epsilon > C_I$. Stability and consistency can then be used to show optimal order convergence of the method in broken energy norm and in $L_2(\Omega)$, see [1].

   A particularly interesting thing about this method is the fact that the inverse inequality (9) is used in a one-sided fashion: the stability only hinges on the shape regularity of $\mathfrak{T}_h^1$. This means that the method is still useful in cases where the mesh $\mathfrak{T}_h^2$ is not shape regular, e.g., when its elements are cut. This fact can be exploited for the construction of overlapping meshes as in [4] or for constructing methods on unfitted meshes as in [2, 3]. Furthermore, it can be used to couple to nonconforming finite element methods on Ω_1 as in [5], or handle a deforming Ω_2 as in [6]. Indeed, many other possibilities remain to be investigated: coupling to meshless methods, to wavelets, or to finite difference methods; coupling of different models as in model reduction methods, etc.

References

[1] R. Becker, P. Hansbo, and R. Stenberg, *A finite element method for domain decomposition with non-matching grids*, M2AN Math. Model. Numer. Anal. **37** (2003), 209–225.

[2] A. Hansbo and P. Hansbo, *An unfitted finite element method, based on Nitsche's method, for elliptic interface problems*, Comput. Methods Appl. Mech. Engrg. **191** (2002), 5537–5552.

[3] A. Hansbo and P. Hansbo, *A finite element method for the simulation of strong and weak discontinuities in solid mechanics*, Comput. Methods Appl. Mech. Engrg. **193** (2004), 3523–3540.

[4] A. Hansbo, P. Hansbo, and M. G. Larson, *A finite element method on composite grids based on Nitsche's method*, M2AN Math. Model. Numer. Anal. **37** (2003), 495–514.

[5] P. Hansbo and J. Hermansson, *Nitsche's method for coupling non-matching meshes in fluid-structure vibration problems*, Comput. Mech. **32** (2003), 134–139.

[6] P. Hansbo, J. Hermansson, and T. Svedberg, *Nitsche's method combined with space-time finite elements for ALE fluid-structure interaction problems*, Comput. Methods Appl. Mech. Engrg. **193** (2004), 4195–4206.

Computing crack propagation by the extended finite element method

Ulrich Hoppe
(joint work with Klaus Hackl, Markus Peters)

Crack propagation is an important process in multi–scale modeling of damage phenomena. Within the finite element method fracture can be modeled in different ways: (i) In a smeared formulation the fracture energy is distributed over the full width of an element or handled by enhanced strain modes, which are discontinuous across element boundaries; (ii) In an interface–element formulation discrete cracks are modeled by special interface–elements along the crack path. This approach usually requires consecutive remeshing; (iii) In the extended finite element method discrete cracks are modeled by enhanced shape–functions. This approach is based on the partition of unity method and is applicable to various kinds of continuum and structural elements in a robust manner [2].

1. Extended Finite Element Method (XFEM)

The XFEM for fracture problems enhances the approximation of the displacement field with discontinuous shape–functions. The enhancement is based on the partition of unity method (PUM), which permits the inclusion of *a priori* knowledge about the differential equation in the ansatz space and allows a construction of ansatz spaces of any desired regularity [1]. A field $u(x)$ is interpolated as

$$(1) \qquad u(x) = \sum_{i=1}^{n} \phi_i(x) \left(a_i + \sum_{j=1}^{m} \psi_j(x) a_{ij} \right),$$

where a_i denote the regular nodal degrees-of-freedom, ψ_j the enhanced basis terms, and a_{ij} the amplitudes of the j-th enhanced basis term at node i. In the special case

of plane fracture problems the displacement field of a body with a one–dimensional discontinuity Γ_d (Fig. 1(a)) is described by

$$(2) \quad \mathbf{u}(\mathbf{X}, t) = \hat{\mathbf{u}}(\mathbf{X}, t) + \mathcal{H}_{\Gamma_d}[\![\mathbf{u}(\mathbf{X}, t)]\!], \qquad \text{with} \qquad \mathcal{H}_{\Gamma_d} = \begin{cases} 1 & \text{if} \quad \mathbf{X} \in \Omega^+ \\ 0 & \text{if} \quad \mathbf{X} \in \Omega^- \end{cases},$$

where $\mathcal{H}_{\Gamma_d}$ denotes the Heaviside function centered on the discontinuity, $[\![z(x)]\!] = z^+(x) - z^-(x)$ represents the jump of a quantity z across the discontinuity, and $\hat{\mathbf{u}}$ denotes the continuous part of the displacement field.

The discontinuous shape function enhancements are required only at those elements that form the support of the crack. According to (2) the finite element shape–functions at those elements are typically enhanced by a Heaviside function term

$$(3) \qquad \mathbf{u} = \sum_i N_i \mathbf{a}_i + \sum_j \mathcal{H}_{\Gamma_d} N_j \mathbf{b}_j,$$

where $\mathbf{b}_j$ accounts for the displacement jump degrees–of–freedom across the discontinuity and N denotes the finite element shape–functions.

In linear fracture mechanics an additional enhancement is needed, because the stress field exhibits a $\frac{1}{\sqrt{r}}$–singularity near the crack–tip. For example, the stress field for mode I fracture (crack opening) near the crack–tip reads

$$(4) \qquad \begin{Bmatrix} \sigma_x \\ \sigma_y \\ \tau_{xy} \end{Bmatrix} = \frac{K_I}{\sqrt{2\pi r}} \cos(\frac{\varphi}{2}) \begin{Bmatrix} 1 - \sin(\frac{\varphi}{2}) \sin(\frac{3\varphi}{2}) \\ 1 + \sin(\frac{\varphi}{2}) \sin(\frac{3\varphi}{2}) \\ \sin(\frac{\varphi}{2}) \cos(\frac{3\varphi}{2}) \end{Bmatrix},$$

where r and φ denote polar coordinates centered at the crack–tip. The factor K_I gives the overall intensity of the stress intensity for the specific fracture mode. The corresponding displacement field for fracture mode I is given by

$$(5) \qquad \begin{Bmatrix} u \\ v \end{Bmatrix} = \frac{K_I}{2G} \sqrt{\frac{r}{2\pi}} \begin{Bmatrix} (\kappa - \cos\varphi) \cos(\frac{\varphi}{2}) \\ (\kappa - \cos\varphi) \sin(\frac{\varphi}{2}) \end{Bmatrix},$$

where u, v are referred to a coordinate system located at the crack–tip and G, κ are material parameters. Similar functions can be found for fracture mode II (crack sliding). In the XFEM approach the stress singularity is modeled by enhancing the standard displacement field with special base functions F_i that span the function space of the crack–tip displacement field for fracture modes I and II. A typical crack-tip enhancement [2, 3] reads

$$(6) \qquad \mathbf{u} = \sum_i N_i \mathbf{a}_i + \sum_j \sum_k N_j F_k \mathbf{c}_{jk}, \qquad \underline{F}_k = \begin{cases} \sqrt{r} \cdot \sin(\frac{\varphi}{2}) \\ \sqrt{r} \cdot \cos(\frac{\varphi}{2}) \\ \sqrt{r} \cdot \sin(\frac{\varphi}{2}) \cdot \sin(\varphi) \\ \sqrt{r} \cdot \cos(\frac{\varphi}{2}) \cdot \sin(\varphi) \end{cases}.$$

The enrichment is restricted to those nodes that belong to the support of the crack tip. The base functions F_l are formulated in polar coordinates centered at the crack–tip and span the displacement field (Fig. 1(b)).
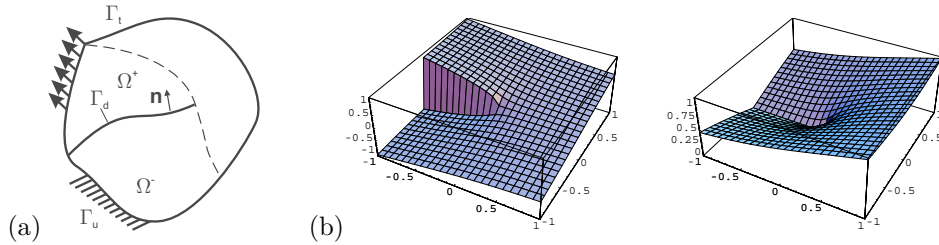
FIGURE 1. (a) Continuous body with discontinuity line; (b) Crack–tip base functions F_1 and F_2

A slight disadvantage of the XFEM is the need for non–standard integration schemes for the enhanced shape-functions. Unfortunately, the standard low or-der Gauss quadrature scheme does not provide accurate results for functions with discontinuous or even singular terms. When almost straight cracks are considered the Gauss quadrature can be applied by subdividing elements into subregions with sufficiently regular functions. But in the vicinity of the crack–tip singularity and along strongly curved crack–paths the subdivision strategy often leads to unde-sirably small sub-elements. To keep control over the accuracy of the integration scheme we have applied an adaptive hierarchical integration algorithm based on Simpson's rule, which provides a natural error indicator [4].
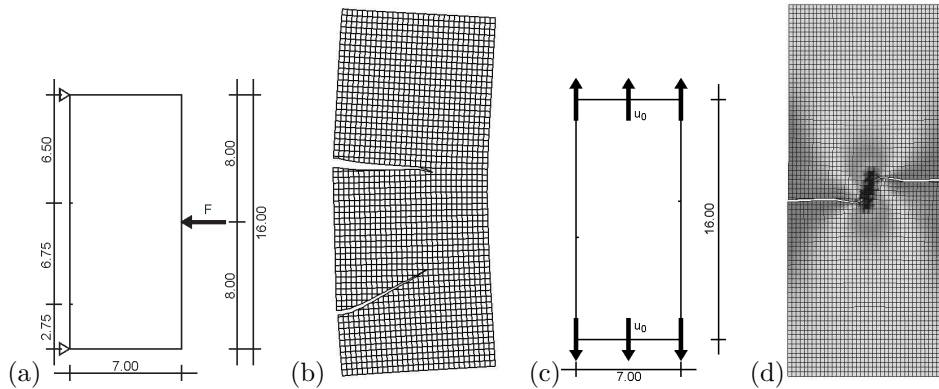
FIGURE 2. Geometries and crack–paths in a three–point bending test and a tension test.

2. EXAMPLES

Figures 2(a,b) show the geometry and the computed crack–paths for a beam under three–point bending. Two initial cracks are prescribed on the left edge of the body and propagate toward the concentrated load along a curved crack–path. Figures 2(c,d) show the geometry and the principal stress contour of a

tension strip with two cracks initiated on opposite edges. The kidney–shaped stress concentration field in front of the crack–tip can be observed.

REFERENCES

[1] J.M. Melenk, I. Babuska, *The Partition of Unity Finite Element Method: Basic Theory and Applications* Comput. Meths. Appl. Mech. Engrg., 139 (1996), 289-314

[2] T. Belytschko and T. Black, *Elastic Crack Growth in Finite Elements With Minimal Remeshing*, International Journal for Numerical Methods in Engineering **45** (1999)

[3] N. Moës, J. Dolbow and T. Belytschko, *A Finite Element Method for Crack Growth without Remeshing*, International Journal for Numerical Methods in Engineering **46** (1999)

[4] M. Peters, U. Hoppe and K. Hackl, *Simulation of crack-propagation using embedded discontinuities*, Proceedings of the Second International Conference Lifetime-Oriented Design Concepts, Bochum, Eds.: F. Stangenberg, O.T. Bruhns, D. Hartmann, G. Meschke (2004)

Energy Norm a Posteriori Error Estimation of hp-Adaptive Discontinuous Galerkin Methods for Elliptic Problems

PAUL HOUSTON

(joint work with Dominik Schötzau and Thomas Wihler)

Adaptive finite element methods that are capable of exploiting both local polynomial–degree–variation (p–refinement) and local mesh subdivision (h–refinement) offer greater flexibility and improved efficiency over mesh refinement methods which only incorporate either local mesh subdivision of the computational domain with the degree of the approximating polynomial fixed, or global polynomial degree variation on a fixed coarse mesh.

The aim of this talk is to consider the energy norm *a posteriori* error analysis of the hp–version of the discontinuous Galerkin (DG, for short) finite element method for approximating second–order linear elliptic partial differential equations. In contrast to the approach of Becker *et al.* [2], which is based on employing a suitable Helmholtz decomposition of the error, together with the underlying conservation properties of DG methods, here we present a new technique to derive *a posteriori* error bounds. Indeed, the analysis presented in this talk is based on rewriting the method in a non-consistent manner using lifting operators in the spirit of Arnold *et al.* [1], and employing a decomposition result for discontinuous spaces, cf. [3], for the case of the h–version of the DG method applied to the Stokes problem.

The performance of the proposed error bound within an hp–adaptive mesh refinement procedure will be demonstrated for problems with both smooth and singular analytical solutions. The key step in the design of such an adaptive algorithm is the local decision taken on each element κ in the computational mesh as to which refinement strategy (i.e., h-refinement *via* local mesh subdivision or p-refinement by increasing the degree of the local polynomial approximation) should be employed on κ in order to obtain the greatest reduction in the error per unit cost. Here, the decision as to whether to h–refine or p–refine an element is based

on a new algorithm for Sobolev–index estimation via truncated Legendre series expansions, cf. [4].

References

[1] D.N. Arnold, F. Brezzi, B. Cockburn, and L.D. Marini, *Unified analysis of discontinuous Galerkin methods for elliptic problems,* SIAM J. Numer. Anal. **39** (2001), 1749–1779.

[2] R. Becker, P. Hansbo, and M.G. Larson, *Energy norm a posteriori error estimation for discontinuous Galerkin methods*, Comput. Methods Appl. Mech. Engrg. **192** (2003), 723–733.

[3] P. Houston, D. Schötzau, and T. Wihler, *Energy norm a posteriori error estimation for mixed discontinuous Galerkin approximations of the Stokes problem*, J. Sci. Comput. **22** (2005), 357–380.

[4] P. Houston and E. Süli, *A note on the design of hp–adaptive finite element methods for elliptic partial differential equations*, Comput. Methods Appl. Mech. Engrg. **194** (2005), 229–243.

A non-standard method for approximating the time harmonic Maxwell system

Peter Monk

(joint work with Tomi Huttunen)

The numerical solution of Maxwell's equations in the context of electromagnetic scattering (for example from aircraft) poses several difficulties. For example the scatterer is usually of complicated shape and made of various materials. A volume based approach (like finite elements) can easily handle these difficulties but is then faced with the problem that dispersion error builds up as the electric size of the problem increases. Furthermore the resulting linear system is difficult to solve. The use of special basis functions in the finite element method may improve the dispersion accuracy of the method and may lead to a better conditioned linear system, but then causes difficulties with implementation.

One possible scheme for using special basis functions (in fact plane wave solutions of the Maxwell system) is the Ultra Weak Variational Formulation (UWVF) of Maxwell's equations due to Cessenat and Després [1, 2]. In this presentation we show first show that the UWVF may be derived as a standard flux splitting Discontinuous Galerkin (DG) method [5] but with a special choice of basis functions.

In particular let Ω denote a bounded polyhedral domain in R^3 and suppose we seek to approximate the electric field E and magnetic field H that satisfy the Maxwell system

$$(1) \qquad\qquad -i\omega\epsilon E - \nabla \times H \;=\; 0 \text{ in } \Omega,$$

$$(2) \qquad\qquad -i\omega\mu H + \nabla \times E \;=\; 0 \text{ in } \Omega,$$

where the electromagnetic parameters ϵ and μ have positive and bounded real parts, and the imaginary part of ϵ is non-negative (μ is assumed real). A major limitation of the UWVF is that it is necessary that the parameters be piecewise

constant with respect to the upcoming finite element mesh. In addition the field satisfies the general boundary condition

(3) $-E \times n + \sigma(H \times n) \times n = Q(E \times n + \sigma(H \times n) \times n) + g$ on $\Gamma = \partial\Omega$

where σ is a positive function of position on the boundary, n is the unit outward normal and g is a tangential data field. The parameter Q is such that $|Q| \leq 1$. Note that $Q = 1$ gives the perfectly conducting boundary condition, while $Q = 0$ gives the impedance boundary condition which includes a simple abosrbing boundary condition.

We shall now derive the UWVF for the basic Maxwell system (1)–(3). Our derivation, which differs from that of Cessenat and Despreés [1, 2], highlights the connection between the UWVF and the classical flux splitting discontinuous Galerkin method for symmetric hyperbolic systems (see for example [5]).

Let $\tau_h = \{K\}$ denote a mesh of finite elements K of maximum diameter h covering Ω. We shall assume that each element K is a tetrahedron and hence has triangular faces (so simplifying some integrals that need to be performed during the calculation).

We now proceed along standard lines to derive a discontinuous Galerkin method for the Maxwell system. For an element K let n^K denote the unit outward normal to the boundary ∂K of K. Now let ξ^K and ψ^K denote smooth vector functions on an element in the mesh. Multiplying (1) and (2) by the complex conjugate of ξ^K and ψ^K and integrating over K using integration by parts identity to move the curl from the trial function to the test function we obtain (the overline denotes complex conjugation):

$$\int_K \left(-i\omega\epsilon E \cdot \overline{\xi^K} - H \cdot \nabla \times \overline{\xi^K}\right) dV = \int_{\partial K} n^K \times H \cdot \overline{\xi^K}\, dA$$

$$\int_K \left(-i\omega\mu H \cdot \overline{\psi^K} + E \cdot \nabla \times \overline{\psi^K}\right) dV = -\int_{\partial K} n^K \times E \cdot \overline{\psi^K}\, dA.$$

Adding the two equations and reordering the left hand side we obtain

$$\int_K \left(E \cdot (\overline{i\omega\epsilon\xi^K + \nabla \times \psi^K}) + H \cdot (\overline{i\omega\mu\psi^K - \nabla \times \xi^K})\right) dV$$

(4)
$$= \int_{\partial K} \left(n^K \times H \cdot \overline{\xi^K} - n^K \times E \cdot \overline{\psi^K}\right) dA$$

where we have used the fact that μ is assumed to be real valued. Usually in the derivation of the discontinuous Galerkin method we would now specify how to compute the "fluxes" or surface currents $n^K \times E$ and $n^K \times H$ from approximate discontinuous fields, but in this case we first make an important assumption that is the essential part of the UWVF. We assume that ξ^K and ψ^K satisfy the following adjoint Maxwell system on K:

(5) $$i\omega\overline{\epsilon}\xi^K + \nabla \times \psi^K = 0 \text{ in } K,$$
(6) $$i\omega\mu\psi^K - \nabla \times \xi^K = 0 \text{ in } K.$$

With this assumption the above identity (4) for (E, H) on K reduces to

$$(7) \qquad \int_{\partial K} \left(n^K \times H \cdot \overline{\xi^K} - n^K \times E \cdot \overline{\psi^K} \right) dA = 0$$

We now apply the usual discontinuous Galerkin upwind splitting method to this identity. Let

$$u^K = \left(\begin{array}{c} E|_K \\ H|_K \end{array} \right) \text{ and } \phi^K = \left(\begin{array}{c} \xi^K \\ \psi^K \end{array} \right)$$

then (7) becomes

$$(8) \qquad \int_{\partial K} D^K u^K \cdot \phi^K \, dA = 0$$

where the matrix D^K is given by

$$D^K = \left(\begin{array}{c|c} 0 & Z^K \\ \hline (Z^K)^T & 0 \end{array} \right) \text{ and } Z^K = \left(\begin{array}{ccc} 0 & n_3^K & -n_2^K \\ -n_3^K & 0 & n_1^K \\ n_2^K & -n_1^K & 0 \end{array} \right).$$

Note that $Z^K a = -n^K \times a$ for any vector a.

Flux splitting amounts to a suitable factoring of D^K into positive and negative semi-definite parts corresponding to left and right going waves. To obtain the general UWVF we use a slightly more general factorization than usual. Let $\sigma > 0$ be defined on the faces of the mesh (on the boundary faces it is the function σ appearing in (3), for other faces it can be taken as the usual impedance). To define the splitting of D^K let

$$L^{K,\pm} = \frac{1}{\sqrt{2\sigma}} \left(\pm\sigma(Z^K)^2, Z^K \right)$$

and define $D^{K,\pm} = \pm(L^{K,\pm})^T(L^{K,\pm})$. A simple calculation then shows that $D^K = D^{K,+} + D^{K,-}$ with $D^{K,+}$ positive semidefinite and $D^{K,-}$ negative semidefinite. An important property of the splitting that we shall use is that if elements K and K' share a common face then on $K' \cap K$ we have (using the fact that $n^K = -n^{K'}$ there)

$$L^{K,+} = \frac{1}{\sqrt{2\sigma}} \left(\sigma(Z^K)^2, Z^K \right) = \frac{1}{\sqrt{2\sigma}} \left(\sigma(Z^{K'})^2, -Z^{K'} \right) = -L^{K',-}.$$

Using the splitting of D^K the factorization of each term in the splitting we may rewrite (8) as

$$(9) \qquad \int_{\partial K} (L^{K,+} u^K) \cdot (L^{K,+} \phi^K) - (L^{K,-} u^K) \cdot (L^{K,-} \phi^K) \, dA = 0$$

The discontinuous Galerkin flux splitting approach is then to couple the solution on adjacent elements using the second term in the above equation. Thus if K' is an element sharing a face with K we have (using the continuity properties of the solutions of Maxwell's equations across an interface in the absence of surface

charges) $L^{K,-}u^K = -L^{K',+}u^{K'}$ on the common face. For faces on the boundary Γ we use the boundary condition (3) written in the convenient form

$$L^{K,-}u^K = QL^{K,+}u^K + \hat{g} \text{ on } \partial K \cap \Gamma$$

where $\hat{g} = -(1/\sqrt{2\sigma})g$. Equation (9) then becomes

$$\int_{\partial K}(L^{K,+}u^K)\cdot(L^{K,+}\phi^K)\,dA + \sum_{K',\partial K'\cap\partial K=f\neq\emptyset}\int_f(L^{K',+}u^{K'})\cdot(L^{K,-}\phi^K)\,dA$$

$$(10) \qquad\qquad + \sum_{\partial K\cap\Gamma=f\neq\emptyset}\int_f(QL^{K,+}u^K+\hat{g})\cdot(L^{K,-}\phi^K)\,dA = 0$$

This is essentially the UWVF of Cessenat and Després before discretization but to make the connection more obvious we define

$$X^K = L^{K,+}u^K|_{\partial K}, Y^K = L^{K,+}\phi^K|_{\partial K} \text{ and } F_K(X^K) = -L^{K,-}\phi^K|_{\partial K}.$$

Then (10) becomes the problem of finding X^K on the face of each element such that

$$\int_{\partial K}X^K\cdot\overline{Y^K}\,dA - \sum_{K',\partial K'\cap\partial K=f\neq\emptyset}\int_f X^{K'}\cdot\overline{F_K(Y^K)}\,dA$$

$$(11)\qquad - \sum_{\partial K\cap\Gamma=f\neq\emptyset}\int_f QX^K\cdot\overline{F_K(Y^K)}\,dA = \int_{\partial K}\hat{g}\cdot\overline{F_K(Y^K)}\,dA$$

for all appropriate Y^K. It turns out that the correct space for X^K and Y^K is the space of square integrable tangential fields on ∂K (see [1]). Equation (11) is the UWVF for Maxwell's equations before discretization. We remark that this derivation of the UWVF extends in a simple way to the equations of elasticity and to the Helmholtz equation written as a first order system (indeed to a general class of symmetric hyperbolic equations).

The UWVF can now be discretized by approximating the function ϕ^K on each element by plane wave solutions of the adjoint Maxwell system (5)-(6). The remainder of the presentation is devoted to showing that techniques for controlling ill-conditioning developed for the Helmholtz equation [4] also can be applied to the Maxwell system. In addition we show that the Perfectly Matched Layer can be implemented for Maxwell's equations by extending the techniques of [3] to this case. Preliminary numerical results also suggest that the PML allows the UWVF to approximate solutions of Maxwell's equations in a layered medium and hence that the UWVF could be used to simulate ground penetrating radar.

References

[1] O. CESSENAT, *Application d'une nouvelle formulation variationnelle aux équations d'ondes harmoniques. Problèmes de Helmholtz 2D et de Maxwell 3D.*, PhD thesis, Université Paris IY Dauphine, 1996.

[2] O. CESSENAT AND B. DESPRÉS, *Using plane waves as base functions for solving time harmonic equations with the Ultra Weak Variational Formulation*, Journal of Computational Acoustics, 11 (2003), pp. 227–38.

[3] T. Huttunen, J. Kaipio, and P. Monk, *The perfectly matched layer for the ultra weak variational formulation of the 3D Helmholtz equation*, Int. J. Numer. Meth. Eng., 61 (2004), pp. 1072–92.

[4] T. Huttunen, P. Monk, and J. Kaipio, *Computational aspects of the Ultra Weak Variational Formulation*, J. Comput. Phys., 182 (2002), pp. 27–46.

[5] P. Lesaint and P. Raviart, *On a finite element method for solving the neutron transport equation*, in Mathematical Aspects of Finite Element Methods in Partial Differential Equations, C. deBoor, ed., Academic Press, New York, 1974, pp. 89–123.

Finite element approximation of saturated/unsaturated flow and reactive solute transport in porous media

Florin A. Radu

(joint work with I.S. Pop, P. Knabner)

Pollution of groundwater by organic compounds is recognized nowadays as a serious and widespread problem. Wherever nocive substances are used or simply deposited it can happen that they come into the soil and through precipitation can reach the groundwater. A reliable prediction of the water movement and solute transport through variably saturated soil, where the chemical species undergo sorption or exchange processes on the surface of the porous skeleton, has a fundamental importance in deciding how dangerous a contaminated site is.

Here, we consider a general mathematical model for coupled flow and reactive solute transport and we briefly describe our numerical approach. A scheme equivalent to the implicit Euler method is used for the discretization in time and the mixed finite element method (MFEM) for the spatial discretization. The main focus is set on the demonstration of the convergence of the fully discrete scheme used for the saturated/unsaturated flow.

The groundwater movement, taking into account the unsaturated subregions near the surface, is described by the Richards' equation, a nonlinear degenerate parabolic partial differential equation

$$(1) \qquad\qquad \partial_t \Theta(\psi) - \nabla \cdot K(\Theta)\nabla(\psi + z) = 0,$$

where ψ is the pressure head, Θ is the water content, K is the hydraulic conductivity and z is the height against the gravitational direction. For the two coefficient functions different models can be choosen to end up with a single unknown in (1). For negative pressure values the nonlinearities are monotone nondecreasing, therefore (1) is a nonlinear parabolic equation there, but positive pressure values lead to a constant value of saturation and represent the region below the groundwater table, where the pressure obeys an elliptic equation. As a consequence we deal with a nonlinear elliptic-parabolic equation whose solution is typically lacking regularity. This and the high nonlinearities appearing in the coefficient functions makes the analysis of numerical schemes for problem (1) generally difficult. A classical trick to combine the two nonlinearities in (1) in just one is to apply the

Kirchhoff transformation

$$(2) \qquad\qquad \mathcal{K} : \mathbb{R} \longrightarrow \mathbb{R}, \psi \longmapsto \int_0^\psi K(\Theta(s))\, ds.$$

By defining now $b(u) := \Theta \circ \mathcal{K}^{-1}(u), k(b(u)) := K \circ \Theta \circ \mathcal{K}^{-1}(u)$ and letting $\mathbf{e_z}$ denote the vertical unit vector, equation (1) becomes

$$(3) \qquad\qquad \partial_t b(u) - \nabla \cdot (\nabla u + k(b(u))\, \mathbf{e_z}) = 0.$$

Due to the above transformation, the diffusion becomes linear in equation (1). However, also after the transformation the equation still remains degenerate and, according to [1], we expect only $\partial_t b(u) \in L^2(0, T; H^{-1}(\Omega))$ which does not allow a mixed variational formulation being the basis for a mixed finite element discretization. To overcome this, the equation (3) is first integrated in time [2, 7, 6]. To the resulting we apply a backward Euler time stepping and MFEM.

Let $\mathcal{T}_h$ be a regular decomposition of the domain $\Omega \subset \mathbb{R}^d$ into closed d-simplices; h stands for the mesh-size. We denote by $W_h \subset L^2(\Omega)$ and $V_h \subset H(\mathrm{div}, \Omega)$ the lowest order finite element spaces of Raviart-Thomas type. Let T be the final time, $N > 1$ an integer giving a time step $\tau = T/N$ and $t_n = n\tau$, $n \in \{1, \ldots, N\}$. At t_n, the *fully discrete mixed variational formulation* of the problem reads as

Let $u_h^{n-1} \in W_h$ be given. Find $(u_h^n, \mathbf{q_h^n}) \in W_h \times V_h$ such that there for all $w_h \in W_h$ and $\mathbf{v_h} \in V_h$ holds

$$(4) \qquad\qquad (b(u_h^n), w_h) + \tau(\nabla \cdot \mathbf{q_h^n}, w_h) \quad = \quad (b(u_h^{n-1}), w_h),$$

$$(5) \qquad (\mathbf{q_h^n}, \mathbf{v_h}) - (u_h^n, \nabla \cdot \mathbf{v_h}) + (k(b(u_h^n))\mathbf{e_z}, \mathbf{v_h}) \quad = \quad 0.$$

The same method has been also analyzed in [2, 6] where similar techniques are used. They consider a time continous semidiscrete scheme as well and prove for it an optimal order of convergence for the L^2-norm of the time integral of the pressure and flux. Unfortunately, for the fully discrete scheme an explicit order of convergence in terms of the discretization parameters τ and h can be obtained only by assuming extra, unrealistic, regularity for the solution (especially for the time derivatives of the pressure and flux).

A very important hint to prove the convergence of the fully discrete scheme (4)–(5), without assuming unrealistic regularity for the solution, was furnished in [3], which deals with a class of multidimensional degenerate parabolic equations including Richards' equation. A fully discrete scheme based on C^0 piecewise linear finite elements is proposed and analyzed. The techniques used here to cope with degenerate parabolic equations will permit us to extend the results in [2] to the general, degenerate case. The idea is to state besides the mixed variational formulations, also suitable continuous and semidiscrete conformal variational formulations for the Richards' equation and to prove their equivalence with the corresponding mixed formulations. In contrast to [2, 6] here the semidiscrete schemes are continuous in space. Then, using specific techniques for conform discretized degenerate parabolic equations [3, 4], we prove error estimates for the continuous

to the semidiscrete step. Next, using the procedure described in [2, 6], error estimates for the semidiscrete to the fully discrete problem can be obtained. Error bounds for the time integral of the flux and of the pressure are derived. In this setting, the equivalence between the two different formulations becomes essential since, in this way, results obtained for the conformal method can be transferred to the mixed one and viceversa. The procedure is detailed presented in [5] (where also a regularization step is performed). By assuming that the flux is in $H^1(\Omega)^d$ instead $H(\text{div}, \Omega)$, which is obviously in the 1D case, our main result reads as

$$(6) \quad \left\| \sum_{n=1}^N \int_{t_{n-1}}^{t_n} (u(t) - u_h^n) \, dt \right\|^2 + \left\| \sum_{n=1}^N \int_{t_{n-1}}^{t_n} (\mathbf{q}(t) - \mathbf{q_h^n}) dt \right\|^2 \leq C(\tau + h^2).$$

We consider now P mobile and M immobile (including microbial populations) species. To describe the transport of the species $i \in \{1, \ldots, P\}$, including the effects of advection, dispersion, sorption and degradation we use the equations

$$(7) \qquad \partial_t(\Theta c_i) + \rho_b \partial_t s_i - \nabla \cdot (\mathbf{D_i} \nabla c_i - \mathbf{q} c_i) = -R_i,$$

with c_i, s_i denoting the concentration of the mobile and the absorbed species, respectively, $\mathbf{D_i}$ the diffusion-dispersion coefficient and ρ_b the bulk density. Here, R_i is the degradation rate which can be a function of all the concentrations appearing in the reaction in which i takes part. The sorption itself is described by

$$(8) \qquad s_i = \phi(c_i) \quad \text{or} \quad \partial_t s_i = k_i(\phi(c_i) - s_i),$$

either as an equibrium or a nonequilibrium process. In (8) ϕ denotes a sorption isotherm and k_i a rate parameter. Finally, we formulate a mass balance to obtain an equation for the evolution of a immobile species

$$(9) \qquad \partial_t c_i + k_{d_i} c_i = R_i, \quad i \in \{P+1, \ldots, P+M\}.$$

with k_{d_i} being the death rate of the microbial population i.

Backward implicit Euler method is used for the temporal discretization and the MFEM is applied for the spatial discretization. Precisely, the lowest order finite elements of Raviart-Thomas type are used for the approximation of the fluxes and piecewise constants for the concentrations. The resulting algebraic system of equations is hybridized by adding Lagrange multipliers on the sides. Briefly, the algorithm reads: within each time step we first solve the Richards equation by a damped Newton's method and then, having computed the water flux and the saturation we solve the fully coupled equations for the species again by a Newton method. Some illustrative numerical examples show that the resulting code can be used as a powerful tool to predict the migration and the extent of contaminant plumes in many case studies.

References

[1] H. W. Alt and S. Luckhaus, *Quasilinear elliptic-parabolic differential equations*, Math. Z. **183** (1983), 311–341.

[2] T. Arbogast, M. F. Wheeler and N. Y. Zhang, *A nonlinear mixed finite element method for a degenerate parabolic equation arising in flow in porous media*, SIAM J. Numer. Anal. **33** (1996), 1669–1687.

[3] R. H. Nochetto and C. Verdi, *Approximation of degenerate parabolic problems using numerical integration*, SIAM J. Numer. Anal. **25** (1988), 784–814.

[4] I. S. Pop, *Error estimates for a time discretization method for the Richards' equation*, Comput. Geosci. **6** (2002), 141–160.

[5] F. Radu, I. S. Pop and P. Knabner, *Order of convergence estimates for an Euler implicit, mixed finite element discretization of Richards' equation*, SIAM J. Numer. Anal. **42**, No. 4 (2004), 1452-1478.

[6] E. Schneid, P. Knabner and F. Radu, *A priori error estimates for a mixed finite element discretization of the Richards' equation*, Numerische Mathematik **98**, No 2 (2004), 353-370.

[7] C. Woodward and C. Dawson, *Analysis of expanded mixed finite element methods for a nonlinear parabolic equation modeling flow into variably saturated porous media*, SIAM J. Numer. Anal. **37** (2000), 701–724.

L^∞-stability of FEM on irregular meshes

Rolf Rannacher

The H_0^1-Ritz projection into finite element subspaces admits order-optimal L^2-error estimates on very general types of meshes. However, corresponding L^∞-error estimates are mostly proven under the more restrictive 'uniform size' and 'uniform shape condition'. Such 'quasi-uniform' meshes occur rather rarely in practice since this condition excludes the appropriate mesh refinement for resolving local singularities and boundary layers. This has raised the question whether local mesh refinement and mesh distortion spoil the overall pointwise convergence of the finite element method. This question is analyzed in Rannacher [9] for the simplest but representative case of P_1-elements on triangular or tetrahedral meshes in two and three dimensions, respectively, for the model problem

$$(1) \qquad -\Delta u = f \quad \text{in } \Omega, \quad u = 0 \text{ on } \partial\Omega,$$

on a (convex) polygonal or polyhedral domain Ω. It is shown that most of the L^∞-stability estimates known for quasi-uniform meshes remain valid in $\mathbb{R}^2$ and with some restrictions also in $\mathbb{R}^3$ for much more irregular meshes. The argument uses the weighted-norm technique introduced in Frehse & Rannacher [3] for proving L^1-error estimates for regularized Green functions. But the reduced regularity assumptions on the meshes require some modifications at critical places.

Let $\{\mathbb{T}_h\}_{h\in\mathbb{R}_+}$ be a family of decompositions $\mathbb{T}_h = \{T\}$ of $\overline{\Omega}$ into (closed) 'cells' (triangles or tetrahedra), such that two adjacent cells only intersect in common vertices, edges or faces. For any $T \in \mathbb{T}_h$, we denote by h_T and ρ_T the radii of the smallest circumscribed and the largest inscribed circle or ball, respectively, and set $h_{\max} := \max_{T\in\mathbb{T}_h} h_T$ and $h_{\min} := \min_{T\in\mathbb{T}_h} h_T$.

Definition 1. *The mesh family* $\{\mathbb{T}_h\}_{h\in\mathbb{R}_+}$ *is said to be 'quasi-uniform' if it satisfies the 'shape-regularity condition',* $h_T \leq c\rho_T, T \in \mathbb{T}_h$, *and the 'size-regularity condition'* $h_{\max} \leq ch_{\min}$, *uniformly for* $h \in \mathbb{R}_+$.

For triangular meshes in $\mathbb{R}^2$ shape regularity is equivalent to the so-called 'minimum angle condition' which requires that all inner angles of the triangles $T \in \mathbb{T}_h$ are uniformly bounded away from zero.

For the subspaces $V_h := \{v_h \in H_0^1(\Omega), v_{h|T} \in P_1(T), T \in \mathbb{T}_h\}$ of P_1-finite elements, the H_0^1-Ritz projection $R_h : V \to V_h$ is defined by

$$(2) \qquad\qquad (\nabla R_h u, \nabla \phi_h) = (\nabla u, \nabla \phi_h) \quad \forall \phi_h \in V_h.$$

For quasi-uniform meshes, we have the usual L^2-convergence estimate

$$(3) \qquad\qquad \|u - R_h u\|_{L^2} + h\|\nabla(u - R_h u)\|_{L^2} \leq ch^2\|u\|_{H^2},$$

which follows by the projection property of the Ritz method and the associated error estimates for the cellwise defined 'nodal interpolation' $I_h : V \cap C^0(\overline{\Omega}) \to V_h$:

$$(4) \quad \|u - I_h u\|_{L^p(T)} + h_T\|\nabla(u - I_h u)\|_{L^p(T)} \leq ch_T^2\|\nabla^2 u\|_{L^p(T)}, \quad d/2 \leq p \leq \infty.$$

It is known that such local estimates also hold on meshes which violate the uniform shape condition in so far that, in $\mathbb{R}^2$, the inner angles of the triangles $T \in \mathbb{T}_h$ are only required to be uniformly bounded away from π; for references see, e.g., Apel & Dobrowolski [1]. Therefore, the L^2-error estimates (3) remains valid even on degenerate meshes satisfying only this so-called 'maximum angle condition'. However, L^∞-error estimates for R_h have usually been proven for quasi-uniform meshes. Under these conditions the (almost) optimal-order L^∞-error estimate

$$(5) \qquad\qquad \|u - R_h u\|_{L^\infty} \leq cL(h)h^2\|u\|_{W^{2,\infty}},$$

was proven first in Natterer [5] and Nitsche [6] and then by various different techniques in Scott [13], Frehse & Rannacher [3] and Schatz & Wahlbin [11]. In these estimates the logarithmic factor $L(h) := |\ln(h)| + 1$ is unavoidable in the case of P_1 elements. These estimates and their variations have important applications in the finite element approximation of strongly nonlinear problems (Frehse & Rannacher [4]), in the analysis of Richardson extrapolation and defect correction (Rannacher [7], [8]) and in the approximation of parameter identification problems with point observations (Rannacher & Vexler [10]).

For non-quasi-uniform meshe one can infer from the analysis in Schatz & Wahlbin [12] that in $\mathbb{R}^2$ the estimate (5) holds on shape regular meshes which satisfy the uniform size condition only in the following weaker sense.

Definition 2. *The family of triangulations* $\{\mathbb{T}_h\}_{h\in\mathbb{R}_+}$ *is said to be 'polynomial size-regular', if there exist an* $\alpha \geq d$, *such that* $\min_{T\in\mathbb{T}_h} |T| \geq ch^\alpha, T \in \mathbb{T}_h, h \in \mathbb{R}_+$.

This condition allows the meshes to be locally refined with polynomial rate towards 'singular' points or edges. It is shown in [9] that most of the above L^∞-results remain valid in $\mathbb{R}^2$ and with some restrictions also in $\mathbb{R}^3$ on 'irregular' meshes characterized by 'polynomial size-regularity' and 'weak form-regularity' in

the sense of the following definition.

Definition 3. *The family of triangulations $\{\mathbb{T}_h\}_{h \in \mathbb{R}_+}$ is said to be 'weakly shape-regular', if each cell $T \in \mathbb{T}_h$ can be mapped to a fixed reference unit-cell $\hat{T}$ by a regular differentiable mapping Φ_T combined with a diagonal scaling $\Lambda = \operatorname{diag}(\lambda_i)$, i.e., $\hat{T} = \Lambda \circ \Phi_T(T)$, where $\|\Phi'(\hat{x})\| \leq c$, $\|\Phi'(\hat{x})^{-1}\| \leq c$ and $\rho_T \leq \lambda_i \leq h_T$, uniformly for $h \in \mathbb{R}_+$ and $T \in \mathbb{T}_h$.*
For triangular meshes in $\mathbb{R}^2$ this is equivalent to the 'maximum angle condition' requiring that all inner angles of $T \in \mathbb{T}_h$ are bounded away from π.

REFERENCES

[1] Apel, T., and Dobrowolski, M.: *Anisotropic interpolation with applications to the finite element method*, Computing 47 (1992), 277–293.

[2] Babuška, I., and Aziz, A. K.: *On the angle condition in the finite element method*, SIAM J. Numer. Anal. 13 (1976), 214-226.

[3] Frehse, J., and Rannacher, R.: *Eine L^1-Fehlerabschätzung für diskrete Grundlösungen in der Methode der finiten Elemente*, Tagungsband Finite Elemente, *Bonn. Math. Schr.* 89 (1976), 92–114.

[4] Frehse, J., and Rannacher, R.: *Asymptotic L^∞-error estimates for linear finite element approximations of quasilinear boundary value problems*, SIAM J, Numer. Anal. 15 (1978), 418–431.

[5] Natterer, F.: *Über die punktweise Konvergenz finiter Elemente*, Numer. Math. 25 (1975), 67-77.

[6] Nitsche, J. A.: *L^∞-convergence of finite element approximation*, Second Conf. on Finite Elements, Rennes, France, 1975.

[7] Rannacher, R.: *Extrapolation techniques in the finite element method (A survey)*, Proc. Summer School on "Numerical Analysis", Helsinki 1987 (O. Nevanlinna, ed.), pp. 80-113, Helsinki University of Technology, Report-MAT-C7 1988.

[8] Rannacher, R.: *Defect correction techniques in the finite element method*, Proc. Conf. on Progress in Partial Differential Equations: The Metz Surveys (M. Chipot, J. Saint Jean Paulin, eds.), pp. 184-200, Longman, 1991.

[9] Rannacher, R.: *On the L^∞ stability of the finite element method on irregular meshes*, Preprint, March 2005.

[10] Rannacher, R., and Vexler, B.: *A priori error estimates for the finite element discretization of elliptic parameter identification problems with pointwise measurements*, to appear in SIAM J. Control Optim., 2005.

[11] Schatz, A. H., and Wahlbin, L. B.: *Interior maximum norm estimates for finite element methods*, Math. Comp. 31 (1977), 414–442.

[12] Schatz, A. H., and Wahlbin, L. B.: *Maximum norm estimates in the finite element method on plane polygonal domains. Part I*, Math. Comp. 32 (1978), 73-109.

[13] Scott, R.: *Optimal L^∞ estimates for the finite element method on irregular meshes*, Math. Comp. 30 (1976), 681-698.

Discontinuous Galerkin Methods and Plasticity: Work in Progress

B. Daya Reddy

(joint work with Jules K. Djoko)

The initial-boundary value problem for elastoplasticity takes the form of a variational inequality (VI). The VI is of the first kind, ie. posed on a convex subset of a Hilbert space, if the flow law is expressed as the classical normality law, while it is of the second kind, ie. includes a non-differentiable functional, if the flow law is expressed in the form that uses the dissipation function. This talk is concerned with finite element approximations of the VI of the second kind.

The theory corresponding to classical Galerkin finite element approximations is well established (see [2]), and this talk explores the use of discontinuous Galerkin (DG) finite element methods for this class of problems.

which the use of DG methods would carry the same advantages as those for elliptic equations. After a review of the relevant results for Galerkin finite element approximations for the VI, the extension to interior penalty DG approximations is discussed. It is shown that the extension is straightforward, with results on consistency, stability and convergence mirroring those for elliptic equations [1].

Of greater interest and significance is the application of DG methods to generalizations of the classical theory of plasticity to problems involving gradient plasticity (see, for example, [3]). This extension of the classical theory takes account of the fact that the classical theory is unable to capture adequately phenomena such as shear bands that occur at the microscopic scale. Instead, it is necessary to introduce in the theory a dependence not only on the internal variables, such as plastic strain, but on their higher-order derivatives as well. The DG method is particularly well suited to such situations, in which continuity of the internal variables is not assumed.

Preliminary results on the use of DG approximations of the VI corresponding to a model of gradient plasticity are presented, and the consistency and convergence of the method are discussed. Current work, on the extension to other models of gradient plasticity, their analysis and computational implementation, are sketched.

References

[1] D. N. Arnold, F. Brezzi, B. Cockburn, and L. D. Marini, *Unified analysis of discontinuous Galerkin methods for elliptic problems,* SIAM J. Numer. Anal. **39** (2001), 1749–1779.

[2] W. Han and B. D. Reddy, *Plasticity: Mathematical Theory and Numerical Analysis*, Springer-Verlag, New York (1999).

[3] N. A. Fleck and J. W. Hutchinson, *Strain gradient plasticity*, Advances in Applied Mechanics **33** (1997), 295–361.

A solid-shell finite element formulation – from a mixed method to a reduced integration concept

STEFANIE REESE

The notion solid-shell is commonly used for shell element formulations which include only displacement degrees-of-freedom. In most cases such elements possess eight nodes, i.e. the geometry of a structure in thickness direction is realistically displayed. This property is in particular important for contact simulations. In the present contribution we derive a solid-shell approach for large deformation inelasticity. Alternative concepts for such applications can be found in [1,2]. Starting from a mixed principle two important assumptions are made. First of all the constitutive relation for the first Piola-Kirchhoff stress includes a special ansatz for the dependence on the local surface coordinates. Secondly the Jacobi matrix is everywhere replaced by its value in the centre of the element.

Variational functional. The starting point of the formulation is the two-field functional

$$(1) \qquad g_1\left(\mathbf{u}^h, \mathbf{H}_{\text{enh}}^h\right) \;=\; \int_{B_0^h} \mathbf{P}\left(\mathbf{H}^h\right) : \operatorname{Grad} \delta \mathbf{u}^h \, dV + g_{\text{ext}} = 0$$

$$(2) \qquad g_2\left(\mathbf{u}^h, \mathbf{H}_{\text{enh}}^h\right) \;=\; \int_{B_0^h} \mathbf{P}\left(\mathbf{H}^h\right) : \delta \mathbf{H}_{\text{enh}}^h \, dV = 0$$

where the displacement vector $\mathbf{u}^h$ and the "enhanced" strain tensor $\mathbf{H}_{\text{enh}}^h$ denote the independent variables (see *Simo & Armero* [3]). The term g_{ext} represents the virtual work of the external loading. The tensor $\mathbf{P}^h := \partial W / \partial \mathbf{H}^h = \mathbf{P}(\mathbf{H}^h)$ (W strain energy per reference volume) defines the first Piola-Kirchhoff stress tensor given as a function of the total strain $\mathbf{H}^h = \operatorname{Grad} \mathbf{u}^h + \mathbf{H}_{\text{enh}}^h$ which is additively decomposed into a compatible part $\operatorname{Grad} \mathbf{u}^h$ and an incompatible (or enhanced) part $\mathbf{H}_{\text{enh}}^h$. The index h indicates that the superscripted quantities have already been discretized by a suitable spatial interpolation.

Special treatment of the terms in thickness direction. The ansatz for $\boldsymbol{H}^h$ which is in detail described in *Reese* [4] (with the Voigt notation being indicated by means of italic bold letters) can be decomposed into a part which depends on the local "thickness" coordinate ζ alone and another part which is linear or bi-linear in the two other local "surface" coordinates ξ and η:

$$(3) \qquad \boldsymbol{H}^h = \underbrace{\boldsymbol{H}_0^h + \boldsymbol{H}_{\text{hg}\,\zeta}^h + \boldsymbol{H}_{\text{enh}\,\zeta}^h}_{:= \, \boldsymbol{H}_\zeta^h} + \underbrace{\boldsymbol{H}_{\text{hg}\,\star}^h + \boldsymbol{H}_{\text{enh}\,\star}^h}_{:= \, \boldsymbol{H}_\star^h}$$

Let us first consider purely elastic material behaviour. To arrive at a solid-shell concept we additititively split the strain energy W into one part which depends only on $\mathbf{b}_\zeta = \mathbf{F}_\zeta \, \mathbf{F}_\zeta^T$ where $\mathbf{F}_\zeta$ is the tensor notation of $\boldsymbol{F}_\zeta = \boldsymbol{I} + \boldsymbol{H}_\zeta$ ($\boldsymbol{I}$ Voigt notation of the identity tensor, index h from now on omitted) and another contribution depending on $\boldsymbol{H}_\star$: $W = W_\zeta\left(\boldsymbol{b}_\zeta\right) + W_\star\left(\boldsymbol{H}_\star\right)$. The first summand W_ζ is assumed to have a classical non-linear form, it could e.g. be given as Neo-Hookean strain

energy function. Futher it should be mentioned that the relation $W_\zeta = W|_{\xi=\eta=0}$ holds. For the second summand we write

$$(4) \qquad\qquad W_\star (\boldsymbol{H}_\star) = \frac{1}{2}\, \boldsymbol{H}_\star^T \boldsymbol{A}_{\mathrm{el}}\, \boldsymbol{H}_\star$$

where $\boldsymbol{A}_{\mathrm{el}}$ is the classical elasticity matrix given in a nine-dimensional format. To avoid volumetric locking the Lamé constant Λ is set equal to zero (in $\boldsymbol{A}_{\mathrm{el}}$). The relation (4) can alternatively be represented in the six-dimensional format $W_\star = \frac{1}{2} \boldsymbol{\varepsilon}_\star^T \boldsymbol{C}_{\mathrm{el}}\, \boldsymbol{\varepsilon}_\star$ where $\boldsymbol{C}_{\mathrm{el}}$ is now the six-dimensional elasticity matrix and $\boldsymbol{\varepsilon}_\star^T :=$ $\{H_{11\star}, H_{22\star}, H_{33\star}, H_{12\star} + H_{21\star}, H_{23\star} + H_{32\star}, H_{31\star} + H_{13\star}\}$ an linearized strain measure. Using the additively decomposed form of W together with (4) the first Piola-Kirchhoff stress tensor is finally given by means of

$$(5) \qquad\qquad \boldsymbol{P} = \partial W_\zeta / \partial \boldsymbol{H}_\zeta + \boldsymbol{A}_{\mathrm{el}}\, \boldsymbol{H}_\star := \boldsymbol{P}_\zeta + \boldsymbol{A}_{\mathrm{el}}\, \boldsymbol{H}_\star$$

Inelasticity. The situation becomes more complex in the case of inelastic material behaviour. Restricting ourselves to isotropy it is easily understandable that the first summand of the strain energy, W_ζ, depends on $\mathbf{b}_{e\,\zeta} = \mathbf{F}_\zeta\, \mathbf{C}_i^{-1} \mathbf{F}_\zeta^T$. Here, $\mathbf{C}_i$ is the so-called inelastic right Cauchy-Green tensor and plays the role of an internal variable. It is determined by integrating an evolution equation of the form (I) $\dot{\mathbf{C}}_i = \mathbf{f}\,(\mathbf{C}, \mathbf{C}_i)$ or (II) $\dot{\mathbf{C}}_i = \mathbf{f}\,(\mathbf{C}, \dot{\mathbf{C}}, \mathbf{C}_i)$ depending on whether rate-dependent (I) or rate-independent material behaviour (II) is considered.

Analogous to the choice of W_ζ the second summand now reads $W_\star = \frac{1}{2}\,(\boldsymbol{\varepsilon}_\star - \boldsymbol{\varepsilon}_{\star i})^T \boldsymbol{C}_{\mathrm{el}}\,(\boldsymbol{\varepsilon}_\star - \boldsymbol{\varepsilon}_{\star i})$ where $\boldsymbol{\varepsilon}_{\star i}$ is an inelastic strain measure. It can e.g. be constructed similarly to the Green-Lagrange strain tensor $(\mathbf{E}_i = \frac{1}{2}\,(\mathbf{C}_i - \mathbf{1}))$. Another possibility is the logarithmic form $\ln \sqrt{\mathbf{C}_i}$.

In order to arrive at a computationally efficient and simple finite element technology it is, however, suitable to express $\boldsymbol{P}_\star$ only in terms of $\boldsymbol{H}_\star$. For this purpose we solve the scalar equation

$$(6) \qquad\qquad (\boldsymbol{\varepsilon}_\star - \boldsymbol{\varepsilon}_{\star i})^T \boldsymbol{C}_{\mathrm{el}}\,(\boldsymbol{\varepsilon}_\star - \boldsymbol{\varepsilon}_{\star i}) = \boldsymbol{\varepsilon}_\star^T \boldsymbol{C}_{\mathrm{in}}\, \boldsymbol{\varepsilon}_\star$$

which contains as only unknown the so-called "inelastic" shear modulus μ_{in} (since the Lamé constant has been set equal to zero). The stress is finally computed by means of $\boldsymbol{P} = \boldsymbol{P}_\zeta + \boldsymbol{A}_{\mathrm{in}}\, \boldsymbol{H}_\star$.

Note that the here presented computation of the inelastic shear modulus is new and improves the concept proposed in *Reese* [4,5] where this parameter is determined on the basis of an empirical formula.

Elimination of internal element degrees of freedom. The interpolation of the enhanced part $\boldsymbol{H}_{\mathrm{enh}}$ includes nine internal element degrees of freedom to be determined by means of solving (2) elementwise. Replacing everywhere the Jacobi matrix by its value in the centre of the element we finally arrive at a linear equation for six of the nine unknown element variables. These six variables can be replaced by a linear expression in terms of the nodal element displacements and therefore do not have to be determined explicitly. For the remaining three element variables which are needed to avoid thickness locking a non-linear equation is derived which must be solved iteratively. In the case of thin structures thickness

locking does not play any role, the three "non-linear" enhanced degrees-of-freedom can be neglected.

Reduced integration with hourglass stabilization. The main step is to exploit the global weak form (1). Without any further assumption the use of the stress relation $\boldsymbol{P} = \boldsymbol{P}_\zeta + \boldsymbol{A}_{\text{in}} \boldsymbol{H}_\star$ leads to the element contribution (index e) $g_1^e = \delta \boldsymbol{U}_e^T \left(\boldsymbol{R}_u^0 + \boldsymbol{R}_u^{\text{hg}} + \boldsymbol{K}_{\text{stab}} \boldsymbol{U}_e \right)$. In the latter relation $\boldsymbol{R}_u^0$ is the constant part of the residual force vector. $\boldsymbol{R}_u^{\text{hg}}$ is ζ-dependent. It can be determined by means of a Gauss point integration in ζ-direction (two Gauss points are usually sufficient). $\boldsymbol{K}_{\text{stab}}$ is the so-called hourglass stabilization matrix which is again constant within the element and can therefore be evaluated in a separate subroutine outside of the Gauss point loop. The form of $\boldsymbol{K}_{\text{stab}}$ is very similar to the one of the element stiffness matrix in linear elasticity. However, we work with a much more sophisticated nine-dimensional form of the "$\boldsymbol{B}$" operator and the linear elasticity matrix is replaced by $\boldsymbol{A}_{\text{in}}$ (see [5]).

Elimination of shear locking. Let us for the following analysis take into account two different shear terms ($C_{\text{in}\,44} = \mu_{\text{in}}$, $C_{\text{in}\,55} = C_{\text{in}\,66} = b\,\mu_{\text{in}}$) in the elasticity matrix ($b \neq 0$). An eigenvalue analysis at the element level for an rectangular element shape (thickness T, length L, width D) shows that certain eigenvalues go to infinity if the ratio $(L\,D)/T^2$ approaches infinity. These expressions are proportional to $b\,\mu_{\text{in}}$. In order to avoid the non-physical increase of these terms b is set equal to $T^2/(L\,D)$ where T is in general the smallest dimension of the element and $L\,D$ the product of the other two.

Summary. Numerical examples show that the new element formulation is well suited for the computation of sophisticated shell problems. Locking is avoided completely. The disadvantage of the former version of the element (documented in [5]) is now overcome by a consistent derivation of μ_{in}.

REFERENCES

[1] R. Hauptmann, K. Schweizerhof, S. Doll, *A systematic development of "solid-shell" element formulations for linear and non-linear analyses employing only displacement degrees of freedom*, International Journal for Numerical Methods in Engineering **42** (2000), 49–69.

[2] A. Legay, A. Combescure, *Elastoplastic stability analysis of shells using the physically stabilized finite element SHB8PS*, International Journal for Numerical Methods in Engineering **57** (2003), 1299–1322.

[3] J.C. Simo, F. Armero & R.L. Taylor, *Improved versions of assumed enhanced strain trilinear elements for 3D finite deformation problems*, Computer Methods in Applied Mechanics and Engineering **110** (2000), 359–386.

[4] S. Reese, *On a physically stabilized one point finite element formulation for three-dimensional finite elasto-plasticity*, to be published in Computer Methods in Applied Mechanics and Engineering (2005)

[5] S. Reese, *A large deformation solid-shell concept based on reduced integration with hourglass stabilization*, submitted to International Journal for Numerical Methods in Engineering (2005)

Discontinuous Finite Elements with Mixed and Hybrid Variables for Elliptic and Advective–Diffusive Problems

Riccardo Sacco

(joint work with Carlo L. Bottasso, Paola Causin)

The object of the presentation is to discuss and analyze a novel finite element formulation, namely, the Discontinuous-Petrov-Galerkin (DPG) method, for the numerical approximation of elliptic [4, 6] and advective-diffusive boundary value problems [5, 3].

Following the typical strategy of Discontinuous Galerkin (DG) methods [1, 2], the DPG procedure emanates from a one-element weak formulation of the differential problem. At this level, two sets of variables are introduced, namely, mixed variables (defined in the interior of each element) and boundary variables (defined on element interfaces).

The interface variables are suitable Lagrangian multipliers that enforce interelement continuity of the solution and of its normal derivative, thus providing the proper connection between neighboring elements. The internal variables allow to weakly satisfy both constitutive and equilibrium relatons, and can be eliminated in favor of the interface variables using static condensation to end up with a system of reduced size in the sole Lagrangian multipliers.

A stability and convergence analysis of the novel formulation are carried out for both elliptic and advective-diffusive model problems. For these latter problems, some emphasis is devoted on the introduction and discussion of a proper stabilization mechanism within the plain DPG formulation in order to cope with advection-dominated flows. The properties of the resulting scheme are examined, and it is shown how to end up with a monotone formulation satisfying a discrete maximum principle irrespective of the value of the Péclet number.

Finally, numerical tests on several benchmark problems with strongly varying coefficients and with steep interior and boundary layers are presented and illustrated to validate the stability and convergence performance, as well as the flux-conservation properties of the DPG method.

References

[1] D. N. Arnold, F. Brezzi, B. Cockburn, L. D. Marini, *Discontinuous Galerkin Methods*, Lecture Notes in Computational Science and Engineering, **11**, Springer, pp. 89–101 (2000).

[2] D. N. Arnold, F. Brezzi, B. Cockburn, L .D. Marini, *Unified Analysis of Discontinous Galerkin Methods for Elliptic Problems*, Penn State Univ. Tech Report no. AM233 (2001).

[3] C. L. Bottasso, P. Causin, R. Sacco, *Flux-Upwind Stabilization of the Discontinuous Petrov-Galerkin Formulation with Lagrangian Multipliers for Advection-Diffusion Problems*, Rapport de Recherche INRIA nr. 5157 (03/2004). Under review on Mathematical Modelling and Numerical Analysis.

[4] C. L. Bottasso, S. Micheletti, R. Sacco, *The Discontinuous Petrov-Galerkin Method for Elliptic Problems*, Comput. Methods Appl. Mech. Engrg., **191**, 3391–3409 (2002).

[5] C. L. Bottasso, S. Micheletti, R. Sacco, *A multiscale formulation of the Discontinuous Petrov–Galerkin Method for Advective-Diffusion Problems*, MOX-Report No. 20, May 2003, to appear in Computer Methods in Applied Mechanics and Engineering.

[6] P. Causin, R. Sacco, *A discontinuous Petrov–Galerkin method with Lagrangian multipliers for second order elliptic problems*, MOX-Report No. 19, May 2003, to appear in SIAM J. Numer. Anal..

Thin Structures with Enhanced High Order Elements

Joachim Schöberl

Enhanced Assumed Strain (EAS) elements have been introduced to avoid volume and shear locking problems, and are commonly used nowadays [1, 5, 2]. We consider the EAS technique as a convenient implementation method for realizing selective projection operators.

EAS elements for beam and plate models are presented. In particular, we discuss high order triangular plate elements based on a stabilization method by Chapelle and Stenberg [3]. Their element is of order $p+1$ for the vertical deflection, and of order p for the rotations (plus some bubbles). Their reduction operator is an L_2-projection into P^{p-1} of the main part of the shear term. Thus, the projection can be realized by the EAS technique. We propose the following modification: Choose order $p + 1$ for the deflection w, but relax the continuity across edges to $[w] \perp P^p$, where $[w]$ denotes the jump. The additional consistency error is bounded by $ch^p(h + t)$, and thus optimal for the range $t \leq h$. The advantage of this modification is that the global shape functions are the same for the deflection and the rotations.

The kinematics of the plate element is translated to anisotropic 3D elements. Since the global basis functions are the same for the deflection and for the rotations, the same global basis functions can be used for all three components of the displacement vector, what is important for curved elements and non-linear elasticity. This is because the normal displacement of the mapped element is not anymore the normal displacement of the reference element.

We present domain decomposition preconditioners which are robust in the plate thickness. The key for the analysis are Fortin operators, which are robust interpolation operators available for the reduced shear energy formulation. The relation of Fortin operators and robust preconditioning was developed in [4].

Numerical examples for Reissner Mindlin plates as well as flat and curved 3D structures are presented.

References

[1] U. Andelfinger and E. Ramm, *EAS-elements for two-dimensional, three-dimensional, plate and shell structures and their equivalence to HR elements.* Int. J. Num. Meth. Eng. **36** (1993), 1311-1337.

[2] D. Braess, C. Carstensen, and D. Reddy., *Uniform convergence and a posteriori error estimators for the enhanced strain finite element method* Numer. Math. **96** (2004), 461-479.

[3] D. Chapelle and R. Stenberg, *An optimal low-order locking-free finite element for Reissner-Mindlin plates*, Math. Models. Meth. Appl. Sciences **8** (1998), 407-430.

[4] J. Schöberl, *Robust Multigrid Methods for Parameter Dependent Problems*, PhD Thesis, 1999, Johannes Kepler University Linz, Austria.

[5] J.C. Simo and S. Rifai. *A class of mixed assumed strain methods and the method of incompatible modes*, Int. J. Num. Meth. Eng. **29** (1990), 1595-1638.

New Research Results on Leibniz' Calculating Machines
Erwin Stein

The lecture starts with an overview of new developments in philosophy, mathematics and natural science in the 17th century, the cradle of modern science and technology, with the beginning age of enlightenment based on a new understanding of our world and the universe in the foregoing renaissance. Important new developments in the 17th century are:

(i) The paradigmatic change from the ancient 'philosophia naturalis' - as deduced from the Aristotelian school and valid until the late scholastics - into new abstract physical theories based on consistent explanations and physical laws of axiomatic character, originating from theory-guided experiments and related measurements, as postulated and achieved by Galileo Galilei in his 'Discorsi' and brought to a first summit by Isaac Newton in his 'Principia'; herein the 'mechanica practica of the 'old' is replaced by the 'mechanica rationalis' - the rational mechanics.

(ii) The invention of analytical geometry by René Descartes and the infinitesimal calculus by Isaac Newton and Gottfried Wilhelm Leibniz

(iii) The theory of determinants by Leibniz using combinatorics and with this the capability of solving algebraic equations and calculating power series, e.g.

Leibniz' ambitions for inventing, constructing and building principally new mechanical calculating machines are additionally motivated by his challenging project of a 'universal science, the 'scientia generalis' based on a new universal, logically consistent scientific language without contradictions, the 'characteristica universalis' in connection with the 'ars inveniendi', thus enabling a general 'calculus logicus'. This program was intended to be developed and applied in existing and new scientific societies, with the guiding goals 'theoria cum praxi' and 'commune bonum' in order to promote science, economics and culture and moreover to improve the condition of life for individuals and societies.

Without knowing the 'Pascaline' of Blaise Pascal from 1644 for adding and subtracting, Leibniz designed his first 'four-species- decimal calculating machine' for adding, multiplication, subtracting and dividing in 1673 in Paris with 4/3/7 places, constructed with an axially movable carriage from place to place, moved by a drawing spindle, and pin-wheels with radially outwards displaced cogs for the input numbers as well as twin horn wheels between the pinwheel shafts which are essential for the decimal carry. The 7 place result device with decimal carries consists of:

- recording gear wheels on the shafts of the recording wheels, driven by the pin wheels
- single-horn wheels on the shafts of the recording wheels
- counting wheels on the shafts of the recording wheels with double functions: (i) as dwelt notches for the result shafts, and (ii) for driving the result wheels via five-bay wheels, thus completing the decimal carry
- intermediate shafts above the twin-horn wheels with five-bay wheels, five-horn wheels and dwelt-notched wheels, each driven by a single horn in front of a five-bay wheel.

This machine didn't work successfully when first presented at the London Royal Society in 1673 but appeared very impressive due to the completely new ingenious and comprehensive concept. Unfortunately, this machine got lost.

From 1693 until the end of his life in 1716, he designed and got built by different mechanicians two new - so called big - machines with axially movable stepped drums instead of the former pin wheels, having 8 input-, 8 counting- and 16 result-places. One of these machines - originating from about 1695 - survived and is owned by the Library of Lower Saxony in Hanover, Germany, which originates from Leibniz' library after his death.

In the 80ies of the 20th century Nikolaus J. Lehmann, Technical University of Dresden, built three replicas of Leibniz' late machine with an important correction and improvement of the decimal carry by sequentially decreasing angles between the two cogs of the twin horns by $35°$ each from right to left places with a maximal angle of $171°$ at the rightest (1st) input place and a minimum angle of $-171°$ at the leftest (8th) input place. The twin horn angles of the original Leibniz machine are $90° \pm 4°$ and thus do not yield correct decimal carries in the full available number set in case of 8 input places. In 2004, Franz Otto Kopp and the author discovered the necessity of rotating the magna rota crank (for adding or subtracting) beyond a full $360°$ rotation with a distinct angle for completing the full decimal carry over 8 places in the general case - if the calculating machine is strictly conceived as a kinematic chain (a gear) with one rotational degree of freedom, i.e. without taking into account free play due to imperfections (as defined by Meyer zur Capellen) and pressing the cogs into dwelt notches of dwelt-notched wheels at about $12°$ from $36°$ for a decimal digit by pressures onto the cog flanges. In a research project of Karl Popp and the author, supported by the German Research Foundation (DFG), a new robust four function machine was designed and built with 6/6/12 places in the scale 2:1 as well as the two important parts 'stepped drum' and 'decimal carry' in the scale 8:1 with all necessary corrections and some partial optimizations, yielding the additional necessary magna rota rotation of $87°$ for 8 input places. This necessary angle is restricted by an admissible angle, determined by a further adding or subtracting operation as well as - less sensitive - a further counting of the number of operations. Unfortunately, this admissible angle is clearly smaller than the necessary one in Leibniz' and Lehmann's machines. One can conclude that we have designed and built in 2004/2005 the first replica of

the four-species Leibniz machine which is fully functioning in the given number set.

Furthermore, a new functional model of Leibniz' 'machina arithmeticae dyadicae', described in 1679, - with a carriage gliding on the double skew plane of the result device - with 7/5/12 places for adding and multiplying - was designed in 2004 by Gerhard Weber and the author and built by Gerhard Weber, based on the first design by Ludolf von Mackensen in 1669 and built in 1971 at the Deutsches Museum Muniche. The new transparent and fully functioning machine has a robust construction of the release mechanism for the binary carry, using balance springs and guideways for the down-rolling metal spheres, optimized inclinations of the skew operating plane, a new closed transport system for the metal spheres and indications for input and result data by rotating flags. the new construction avoids the crucial problem of conflicts (jams) of spheres released from binary carries with new down-rolling spheres according to the input data.
Both new machines fulfill the postulate for our Hanover Leibniz Exhibition: 'Leibniz for touching and understanding'.

REFERENCES

[1] F.-O. Kopp, E. Stein, K. Popp, *N*eue Forschungsergebnisse und Nachbauten zu den Leibnizschen Rechenmaschinen, submitted for publication to 'Studia Leibniziana of the Leibniz-Gesellschaft Hannover in 2005.

Novel FE Discretization Methods for the Computation of Strong and Weak Discontinuities at Finite Strains

PAUL STEINMANN

(joint work with Julia Mergheim)

In the present contribution a discontinuous finite element method for the computational modelling of strong and weak discontinuities in geometrically nonlinear elasticity is introduced. Thereby we denote with 'strong discontinuities' jumps in the deformation map, for example cracks, and with 'weak discontinuities' jumps in the deformation gradient, which occur e.g. at material interfaces. The location of the interface is independent of the mesh structure and therefore discontinuous elements are introduced, to capture the jump in the deformation map or its gradient, respectively. The presented method is closely related to the approach suggested by Hansbo and Hansbo in [1] and [2], where an unfitted finite element method was introduced to simulate strong and weak discontinuities, by means of an extended version of Nitsche's method [3].
In the present approach a variational formulation based on the principle of stationary potential energy is derived for both, the modelling of strong and weak discontinuities. To model strong discontinuities the cohesive crack concept is adopted. The inelastic material behaviour is covered by a cohesive constitutive law, which associates the cohesive tractions, acting on the crack surfaces, with the jump in

the deformation map.

If weak discontinuities, for example material interfaces or inclusions, are considered, the deformation map shall be continuous but its gradient can posses a jump along the interface. Since the same discontinuous elements are used, the continuity of the deformation map has to be ensured. Therefore a finite element method, based on Nitsche's method, for geometrically nonlinear elasticity is formulated. By means of Nitsche's method the continuity of the deformation map is ensured in a weak sense, but the discontinuous element formulation allows for jumps of its gradient.

We consider a body $\mathcal{B}$ which is divided by a discontinuity Γ into the parts $\mathcal{B}^1$ and $\mathcal{B}^2$. The associated normal vector $\boldsymbol{N}$ points from $\mathcal{B}^2$ to $\mathcal{B}^1$. We consider a nonlinear and non-continuous deformation map $\boldsymbol{\varphi}$, which maps the body from the reference configuration to its spatial configuration. The deformation map as well as its gradient and the related strain measures are defined separately for each continuous part of the body

$$(1) \qquad \boldsymbol{\varphi}(\boldsymbol{X}) = \left\{ \begin{array}{lll} \boldsymbol{\varphi}^1(\boldsymbol{X}) & : & \mathcal{B}^1 \to \mathcal{S}^1 \\ \boldsymbol{\varphi}^2(\boldsymbol{X}) & : & \mathcal{B}^2 \to \mathcal{S}^2 \end{array} \right. \qquad \boldsymbol{F} = \left\{ \begin{array}{lll} \boldsymbol{F}^1 & = & \nabla_{\boldsymbol{X}} \boldsymbol{\varphi}^1 \\ \boldsymbol{F}^2 & = & \nabla_{\boldsymbol{X}} \boldsymbol{\varphi}^2. \end{array} \right.$$

The variational formulation, concerning strong discontinuities, is given by

$$(2) \quad \delta\Pi(\boldsymbol{\varphi}, \delta\boldsymbol{\varphi}) = \int_{\mathcal{B}} \delta\boldsymbol{F} : \boldsymbol{P} \, dV + \int_{\Gamma} [\![\delta\boldsymbol{\varphi}]\!] \cdot \bar{\boldsymbol{t}}_0([\![\boldsymbol{\varphi}]\!]) \, d\bar{A} - \int_{\partial\mathcal{B}_N} \delta\boldsymbol{\varphi} \cdot \boldsymbol{t}_0 \, dA = 0,$$

whereby $\boldsymbol{P}$ denotes the Piola stress tensor, which is derived from the strain energy function by $\boldsymbol{P} = \partial\Psi(\boldsymbol{F})/\partial\boldsymbol{F}$. The additional interfacial contribution is due to the cohesive traction vector $\bar{\boldsymbol{t}}_0 = \partial\bar{\Psi}([\![\boldsymbol{\varphi}]\!])/\partial[\![\boldsymbol{\varphi}]\!]$, which is calculated as the derivative of the cohesive potential with respect to the jump in the deformation map.

For the bulk material we assume hyperelastic material behaviour of a compressible Neo-Hooke type. Since we want the cohesive potential to depend only on the jump in the deformation map, we introduce the following cohesive potential which leads to the traction-separation law and results in a symmetric formulation

$$(3) \qquad \bar{\Psi}([\![\boldsymbol{\varphi}]\!]) = \frac{\alpha}{\beta} \left[1 - \exp\left(-\beta \, |[\![\boldsymbol{\varphi}]\!]|\right) \right] \qquad \bar{\boldsymbol{t}}_0 = \alpha \, \exp\left(-\beta \, |[\![\boldsymbol{\varphi}]\!]|\right) \frac{[\![\boldsymbol{\varphi}]\!]}{|[\![\boldsymbol{\varphi}]\!]|}.$$

Thereby α and β are material parameter.

The variational formulation for the case of weak discontinuities contains additional interfacial contributions due to Nitsche's method and is introduced as

$$\delta\Pi(\boldsymbol{\varphi}, \delta\boldsymbol{\varphi}) = \int_{\mathcal{B}} \delta\boldsymbol{F} : \boldsymbol{P} dV + \int_{\Gamma} [\![\delta\boldsymbol{\varphi}]\!] \cdot \{\boldsymbol{P}\} \cdot \boldsymbol{N} d\bar{A} + \int_{\Gamma} [\![\boldsymbol{\varphi}]\!] \cdot \{\mathbf{A} : \delta\boldsymbol{F}\} \cdot \boldsymbol{N} d\bar{A}$$

$$(4)$$

$$+ \int_{\Gamma} \theta \, [\![\delta\boldsymbol{\varphi}]\!] \cdot [\![\boldsymbol{\varphi}]\!] d\bar{A} - \int_{\partial\mathcal{B}_N} \delta\boldsymbol{\varphi} \cdot \boldsymbol{t}_0 \, dA = 0,$$

whereby the tangent operator $\mathbf{A}$ is calculated as the second derivative of Ψ with respect to $\boldsymbol{F}$. The scalar θ is a penalty parameter, which depends on the discretization and has to be sufficiently large to assure the stability of the method.

The weak governing equations are solved using finite elements which allow for a
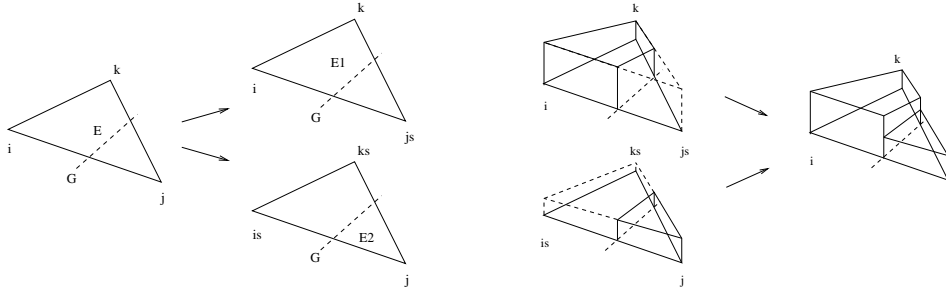
FIGURE 1. Split of linear triangular element

jump in the deformation map. In the discontinuous elements additional displacement degrees of freedom are introduced at the existing nodes. Two independent copies of the standard basis functions are used, one set is put to zero on one side of the discontinuity, while it takes its usual values on the opposite side, and vice versa for the other set. Figure (1) highlights the construction of a discontinuous linear triangular element.

Finally the applicability of the method for the mesh-independent modelling of strong and weak discontinuities is highlighted by means of numerical examples. For the simulation of strong discontinuities a stress-based crack propagation criterion is adopted. As representative examples a symmetric peel test is considered, see figure (2) and a plate with a soft circular inclusion, compare figure (3). The
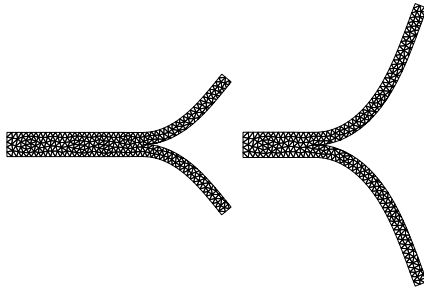
FIGURE 2. symmetric peel test
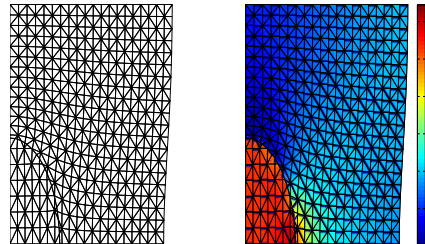
FIGURE 3. deformation and strain in a plate with soft circular inclusion

present approach can be considered as a methodically unified framework for the modelling of strong and weak discontinuities, since the same discretization is used, which implies the formulation of the discontinuous elements, and the variational

formulations differ only in the additional interface contributions due to the cohesive crack concept and Nitsche's method respectively.

REFERENCES

[1] A. Hansbo and P. Hansbo. An unfitted finite element method, based on Nitsche's method, for elliptic interface problems. *Computer Methods in Applied Mechanics and Engineering*, 191:5537–5552, 2002.

[2] A. Hansbo and P. Hansbo. A finite element method for the simulation of strong and weak discontinuities in solid mechanics. *Computer Methods in Applied Mechanics and Engineering*, 193:3523–3540, 2004.

[3] J. Nitsche. Über ein Variationsprinzip zur Lösung von Dirichlet-Problemen bei Verwendung von Teilräumen, die keinen Randbedingungen unterworfen sind. *Abh. Math. Univ. Hamburg*, 36:9–15, 1970.

Formulation of robust shell elements on the basis of mixed variational principles

WERNER WAGNER

(joint work with Friedrich Gruttmann)

In this paper a refined quadrilateral shell element based on a mixed formulation is presented. Assuming a Reissner–Mindlin kinematic with inextensible director the shell strains are derived from the Green–Lagrangean strain tensor and lead to strains $\varepsilon_G(\mathbf{v})$, see e.g. [1], where $\mathbf{v}$ denotes the displacement field. The reference surface of the shell is loaded with surface loads $\bar{\mathbf{p}}$ and boundary loads $\bar{\mathbf{t}}$. Hence the variational formulation is introduced using a Hu–Washizu functional with independent displacements $\mathbf{v}$, strains ε and stress resultants $\boldsymbol{\sigma}$ as follows

$$(1)\quad \Pi(\mathbf{v}, \boldsymbol{\sigma}, \varepsilon) = \int\limits_{(\Omega)} [W(\varepsilon) + \boldsymbol{\sigma}^T(\varepsilon_G(\mathbf{v}) - \varepsilon)]\, dV - \int\limits_{(\Omega)} \mathbf{v}^T\bar{\mathbf{p}}\, dV - \int\limits_{(\Gamma_\sigma)} \mathbf{v}^T\bar{\mathbf{t}}\, dA \to \text{stat.}$$

The strain energy function W is a function of the independent strain field and is specified for nonlinear elastic and inelastic material behaviour. Thus, the stationary condition is approximated within the finite element method and iteratively solved using Newtons method. For this purpose the position vectors $\mathbf{X}$, $\mathbf{x}$ and the displacement vector $\mathbf{u}$ of the mid-surface as well as the director vectors $\mathbf{D}$ and $\mathbf{d}$ are interpolated with bilinear functions $N_I = 1/4(1 + \xi_I\xi)(1 + \eta_I\eta)$ with $\xi_I \in \{-1,\ 1,\ 1, -1\}$ and $\eta_I \in \{-1, -1,\ 1,\ 1\}$. Based on the shell theory C^0-continuity is assumed for the displacements. The element formulation allows the consideration of finite rotations. For the independent strain ε and stress resultant field $\boldsymbol{\sigma}$ we assume C^{-1}-continuity, which means that associated variables are defined only on element level. The interpolation functions for the membrane forces and bending moments are chosen according to [2]. The independent field of stress

resultants $\boldsymbol{\sigma}$ is approximated as follows

$$\boldsymbol{\sigma}^h = [\mathbf{1}_8, \tilde{\mathbf{N}}_\sigma]\,\hat{\boldsymbol{\sigma}} \qquad\qquad \tilde{\mathbf{N}}_\sigma = \left[\begin{array}{ccc} \mathbf{N}_\sigma^m & \mathbf{0} & \mathbf{0} \\ \mathbf{0} & \mathbf{N}_\sigma^b & \mathbf{0} \\ \mathbf{0} & \mathbf{0} & \mathbf{N}_\sigma^s \end{array}\right]$$

(2)

$$\mathbf{N}_\sigma^m = \mathbf{N}_\sigma^b = \mathbf{T}_\sigma^0 \left[\begin{array}{cc} \eta - \bar{\eta} & 0 \\ 0 & \xi - \bar{\xi} \\ 0 & 0 \end{array}\right] \quad \mathbf{N}_\sigma^s = \tilde{\mathbf{T}}_\sigma^0 \left[\begin{array}{cc} \eta - \bar{\eta} & 0 \\ 0 & \xi - \bar{\xi} \end{array}\right]$$

where the matrices $\mathbf{T}_\sigma^0$ and $\tilde{\mathbf{T}}_\sigma^0$ describe the transformation of contravariant tensor components to the local cartesian coordinate system at the element center using the components $J_{\alpha\beta}^0 = J_{\alpha\beta}(\xi = 0, \eta = 0)$ of the Jacobian matrix $\mathbf{J}$ evaluated at the element center. The constants $\bar{\xi}$ and $\bar{\eta}$ are introduced to obtain decoupled matrices in the mixed formulation and denote the coordinates of the center of gravity of the element. The approximation of the strain field $\boldsymbol{\varepsilon}$ is chosen in a similar way. Restrictions concerning fulfilment of the patch test and stability are discussed. The developed mixed hybrid shell element possesses the correct rank and fulfills the in–plane and bending patch test. For geometrical and material linearity the element matrices can be integrated analytically and lead to a fast and effective stiffness computation, [3]. For the nonlinear case numerical integration is applied. The formulation is illustrated by several numerical examples which include bifurcation and post–buckling response as well as inelastic computations. The essential feature of the new element is the robustness in the equilibrium iterations. It allows very large load steps in comparison to other element formulations.
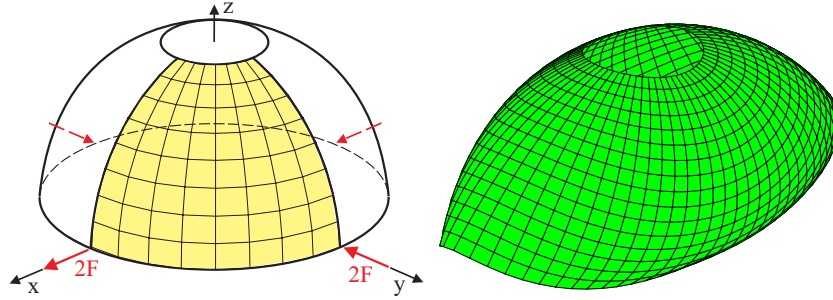
FIGURE 1. Hemispherical shell and deformed mesh for F=100

EXAMPLE: Hemispherical Shell with a 18 hole

The hemispherical shell with a 18 hole under opposite loads is a standard example in linear and nonlinear shell analysis. A quarter of the shell is modelled with 16×16 elements using symmetry conditions, see Fig. 1. The material properties are $E = 6.825 \cdot 10^7$ and $\nu = 0.3$, the radius is $R = 10$ and the thickness is $t = 0.04$. The complete load deflection curve for a 16×16 mesh is presented in Fig. 2. Results for the present element – which are nearly identical with the EAS–shell
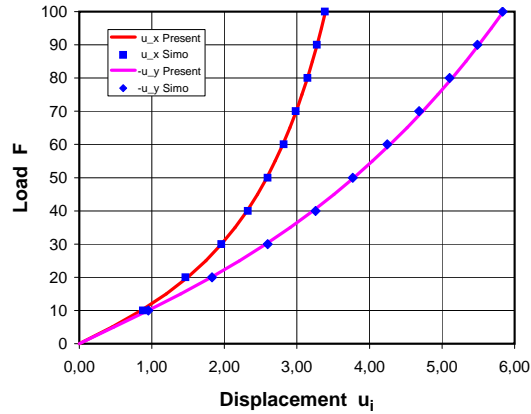
FIGURE 2. Load versus deflection for the hemispherical shell

[4] – show a very good agreement with those reported in [5]. Starting with F=0 a maximum load step of 40 is possible with the EAS–shell [4]. For this load step the norm of the residual vector within the equilibrium iteration is given in Tab. 1 and shows the superior behaviour of the new element. It is important to note that the relative large number of 19 iterations occur for a finite rotation element along with large rigid body motions and is not a consequence of the enhanced strain formulation. Moreover, the total load of 100 can be calculated using the present element in one load step with 17 iterations.

TABLE 1. Comparison of iteration behaviour for load F: $0 \rightarrow 40$

Iterat.	EAS-shell [4]	present element
1	5.6568542E+01	5.6568542E+01
2	2.7885600E+06	2.8374888E+06
3	4.6613004E+05	3.3241348E+05
4	1.9427725E+05	2.4512080E+04
5	6.7170299E+04	2.8536896E+02
6	2.6142653E+04	4.5611620E-02
7	1.3555091E+04	1.5785771E-08
8	3.5529025E+03	
9	5.5833012E+03	
10	9.2807935E+02	
11	4.6902795E+03	
12	2.0239489E+02	
13	2.2367207E+03	
14	1.4962903E+01	
15	2.2588811E+03	
16	9.1847138E-01	
17	1.4030970E+01	
18	5.8607442E-04	
19	9.5610236E-06	

REFERENCES

[1] W. Wagner, F. Gruttmann F, *A Simple Finite Rotation Formulation for Composite Shell Elements*, Eng. Comp., **11** (1994), 145–176.
[2] T.H.H. Pian, K. Sumihara, *Rational approach for assumed stress finite elements*, Int. J. Num. Meth. Eng., **20** (1984), 1685–1695.
[3] F. Gruttmann, W. Wagner, *A linear quadrilateral shell element with fast stiffness computation*, accepted for publication in Comp. Meth. Appl. Mech. Engng., (2005).
[4] R. Sauer, *Eine einheitliche Finite–Element–Formulierung für Stab– und Schalentragwerke mit endlichen Rotationen*, Bericht 4 (1998), Institut für Baustatik, Universität Karlsruhe (TH).
[5] J.C. Simo, M.S. Rifai, D.D. Fox, *On a stress resultant geometrically exact shell model. Part III: Computational aspects of the nonlinear theory*, Comp. Meth. Appl. Mech. Engng., **79**, (1990), 21–70.

Finite-Element Simulation of Failure of Materials under Shock-Loading Conditions

KERSTIN WEINBERG

(joint work with Michael Ortiz and Alejandro Mota)

The goal of our work is to enable finite-element simulations of structural components loaded up to their limit load in a rapid regime. Typical are situations of shock-loaded metals and metal alloys but even human tissue may be subjected to shock waves during medical treatment. In this paper we focus on the simulation of failure of ductile metals. Most metals and alloys contain a certain amount of arbitrarily distributed cavities, with their growth and finally coalescence being the basic failure mechanism in ductile fracture. Typically the size of the cavities (voids) is small compared to the size of the body, and their distribution is defined by a characteristic function $\chi = \chi(x), x \in \mathbb{R}^3$. The spatial average over the current volume of the body V defines the void volume fraction or porosity

$$(1) \qquad\qquad f = \frac{1}{V} \int_V \chi(x)\ dx,$$

which is, for typical engineering materials, initially in the range of 10^{-2} to 10^{-4}. It is known from experiments that the voids start to coalesce and eventually ductile failure occurs when the porosity of the material reaches values from 0.1 to 0.3 (cf. [4] and references therein).

In the following we sketch a variational constitutive model for porous plastic materials under static and dynamic loading conditions. The constitutive framework used here is based on a multiplicative decomposition of the deformation gradient into an elastic part and an inelastic part, and on a conventional internal-variable formulation of continuum thermodynamics. Using a relatively simple dilute model we link the mechanism of plastic expansion and global softening of the material to parameters which describe the micromechanical mechanisms of void growth; avoiding altogether the need of macroscopic failure criteria.

The thermo-mechanical response of the solids considered here is characterized by a free-energy density per unit undeformed volume of the form

$$(2) \qquad A = A(\boldsymbol{F}, \boldsymbol{F}^p, \epsilon^p, \theta^p, T),$$

where $\boldsymbol{F}$ is the deformation gradient, $\boldsymbol{F}^p$ and $\boldsymbol{F}^e = \boldsymbol{F}\boldsymbol{F}^{p-1}$ are the plastic part and the elastic part of the deformation gradient, respectively, $\epsilon^p \geq 0$ is an effective deviatoric plastic strain, $\theta^p \geq 0$ is an effective volumetric plastic strain, T is the absolute temperature. Analogously, the kinetic equations are derived from a rate potential,

$$(3) \qquad \psi^* = \psi^*(\dot{\boldsymbol{F}}^p, \dot{\epsilon}^p, \dot{\theta}^p, T).$$

The plastic deformation rate is assumed to obey the flow rule

$$(4) \qquad \dot{\boldsymbol{F}}^p \boldsymbol{F}^{p-1} = \dot{\epsilon}^p \boldsymbol{M} + \dot{\theta}^p \boldsymbol{N},$$

where $\dot{\epsilon}^p$ and $\dot{\theta}^p$ are subject to the irreversibility constraints

$$(5) \qquad \dot{\epsilon}^p \geq 0, \quad \dot{\theta}^p \geq 0,$$

and the tensors $\boldsymbol{M}$ and $\boldsymbol{N}$ set the direction of the deviatoric and volumetric plastic deformation rates, respectively. They are assumed to satisfy

$$(6) \qquad \mathrm{tr}\boldsymbol{M} = 0, \quad \boldsymbol{M} \cdot \boldsymbol{M} = \frac{3}{2}, \quad \boldsymbol{N} = \pm\frac{1}{3}\boldsymbol{I},$$

with the plus sign in $\boldsymbol{N}$ corresponding to void expansion, and the minus sign to void collapse. The tensors $\boldsymbol{M}$ and $\boldsymbol{N}$ are otherwise unknown and are to be determined as part of the solution. The constraints (6) may be regarded as defining the assumed kinematics of plastic deformation. The direction of plastic deformation, as determined by $\boldsymbol{M}$ and $\boldsymbol{N}$, follows from the variational structure of the constitutive update in a manner which generalizes the principle of maximum dissipation, cf. [2, 3].

For purely volumetric deformations the flow rule (4) reduces to

$$(7) \qquad \frac{d}{dt} \log J^p = \mathrm{tr}\boldsymbol{N}\dot{\theta}^p = \pm\dot{\theta}^p,$$

where J^p is the Jacobian of the plastic deformation gradient, $J^p = \det \boldsymbol{F}^p$. From (7) we find

$$(8) \qquad \dot{\theta}^p = \left| \frac{d}{dt} \log J^p \right|, \quad \theta^p(t) = \theta^p(0) + \int_0^t \dot{\theta}^p(\xi) \, d\xi,$$

i.e., the variable θ^p is a measure of the *accumulated* volumetric plastic deformation. Evidently, θ^p and $\log J^p$ coincide up to a constant for monotonic expansion, but the distinction between the two variables becomes important for arbitrary loading combining alternating phases of void expansion and collapse.

We apply an incremental solution procedure with time intervals $[t_n, t_{n+1}]$. For every $t \in [t_n, t_{n+1}]$ we introduce the power functional

$$
(9) \quad \Phi[\dot{\boldsymbol{\varphi}}, \dot{\epsilon}^p, \dot{\theta}^p, \boldsymbol{M}, \boldsymbol{N}] = \int_B \left[\dot{A} + \psi^* - \left(\frac{\partial L}{\partial \boldsymbol{F}^p} - \frac{d}{dt} \frac{\partial L}{\partial \dot{\boldsymbol{F}}^p} \right) \cdot \dot{\boldsymbol{F}}^p \right] dV -
$$
$$
\int_B \rho_0 (\boldsymbol{B} - \ddot{\boldsymbol{\varphi}}) \cdot \dot{\boldsymbol{\varphi}} \, dV - \int_{\partial_2 B} \bar{\boldsymbol{T}} \cdot \dot{\boldsymbol{\varphi}} \, dS.
$$

where $\boldsymbol{F}^p$, ϵ^p, θ^p, $\boldsymbol{M}$ and $\boldsymbol{N}$ are now regarded as fields over the body B during deformation φ and supposed to body force and surface traction loads $\boldsymbol{B}$ and $\boldsymbol{T}$. The plastic deformation $\dot{\boldsymbol{F}}^p$ is determined by $\dot{\epsilon}^p$, $\dot{\theta}^p$, $\boldsymbol{M}$ and $\boldsymbol{N}$ through the flow rule (4). In difference to the classical (static) approach we assume that the kinetic energy of the body may be written as a sum of the macroscopic inertia and the microinertia attendant to plastic deformation during rapid void growth. The latter, formulated as a function $L = L(\dot{\boldsymbol{F}}^p, \boldsymbol{F}^p)$ induces by variation the term in parenthesis in equation (9). This term may be regarded as an additional stress acting on $\boldsymbol{F}^p$, arising from microinertia. For more details on the variational formulation of the dynamic problem and on the kinematics of void growth we refer to [5].

An example of the capability of the method is the simulation of the forced expansion and ductile fracture and fragmentation of U-6%Nb rings. An outward radial force is applied to the rings by a driver ring, which in turn interacts with a solenoid. When current is applied to the solenoid, a magnetic force is induced in the driver ring creating a sudden uniform radial body force. The rings are thus forced to expand and eventually fracture dynamically. The U-6%Nb rings have an inner diameter of 34.37mm, and a thickness of 0.76mm.

The process is modelled by using the porous plasticity model in conjunction with the strain localization model developed by Yang et al. [6], which is specially well-suited for the simulation of nucleation and propagation of ductile fracture. The finite element mesh used in our simulations is shown in Figure 1 (initially 2634 nodes, 882 tetrahedral elements). The nucleation and propagation of fracture is
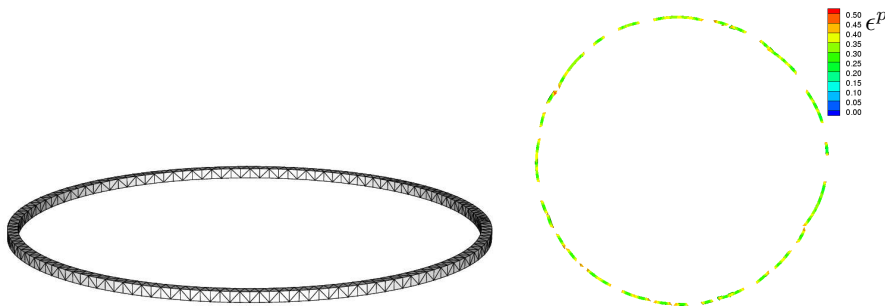
Figure 1. Finite element mesh for the U-6%Nb ring and fragmentation of the ring at 90μs.

simulated by adaptively inserting surface-like strain localization elements between

bulk elements. Figure 1 shows the fragmentation that begins after around 30μs at a final time of 90μs. The number of major fragments obtained in the simulation is 26, compared to 19 fragments as observed in experiments [1].

References

[1] D.E. Grady and D.A. Benson. Fragmentation of metal rings by electromagnetic loading. *Exp. Mech.*, 23(4):393–400, 1983.

[2] K. Hackl. Generalized standard media and variational principles in classical and finite strain elastoplasticity. *J. Mech. Phys. Solids*, 45(5):667–688, 1997.

[3] M. Ortiz and L. Stainier. The variational formulation of viscoplastic constitutive updates. *Comput. Method. Appl. M.*, 171(3-4):419–444, 1999.

[4] V. Tvergaard. Material failure by void growth to coalescence. *Adv. Appl. Mech.*, 27:83–151, 1990.

[5] K. Weinberg, A. Mota, and M. Ortiz. A Variational Constitutive Model for Porous Metal Plasticity *Comp. Mech.*, 2005. to appear.

[6] Q. Yang, A. Mota, and M. Ortiz. A class of variational strain-localization finite elements. *Int. J. Numer. Meth. Eng.*, 2004. submitted.

Mixed finite elements for elasticity; a constructive approach

Ragnar Winther

(joint work with Douglas N. Arnold, Richard S. Falk)

The purpose of this talk is to derive a connection between discrete de Rham complexes and corresponding discrete elasticity complexes, and to utilize this connection to derive new mixed finite elements for linear elasticity.

If Ω is a three dimensional domain then the de Rham complex corresponds to the sequence of maps

$$\mathbb{R} \xrightarrow{\subset} C^\infty \xrightarrow{\text{grad}} C^\infty(\mathbb{R}^3) \xrightarrow{\text{curl}} C^\infty(\mathbb{R}^3) \xrightarrow{\text{div}} C^\infty \longrightarrow 0.$$

Here C^∞ is the space of smooth real valued functions on Ω, while $C^\infty(\mathbb{R}^3)$ denotes the space of smooth functions on Ω with values in $\mathbb{R}^3$. We recall that the statement that this sequence is a complex simply means that the composition of two succeeding maps is identical zero. Furthermore, if Ω is contractible this is an exact complex, i.e., the range of each map is exactly the null space of the succeeding map. A corresponding discrete de Rham complex is of the form

$$\mathbb{R} \xrightarrow{\subset} S_h \xrightarrow{\text{grad}} Z_h \xrightarrow{\text{curl}} V_h \xrightarrow{\text{div}} Q_h \longrightarrow 0,$$

where the spaces S_h, Z_h, V_h, and Q_h are suitable finite element spaces.

It is well–known by now that there is a close connection between discrete de Rham complexes and the construction of mixed finite element methods for second order elliptic problems. It can be argued that there is a similar connection between mixed finite element methods for elasticity, i.e., methods derived from the Hellinger–Reissner variational principle, and a corresponding elasticity complex. This complex takes the form

$$RM \xrightarrow{\subset} C^\infty(\mathbb{R}^3) \xrightarrow{\epsilon} C^\infty(\mathbb{S}) \xrightarrow{J} C^\infty(\mathbb{S}) \xrightarrow{\text{div}} C^\infty(\mathbb{R}^3) \longrightarrow 0.$$

Here RM is the six dinensional space of rigid motions, and $C^\infty(\mathbb{S})$ denotes the space of smooth maps on Ω with values in the set of symmetric matrices, $\mathbb{S}$. The operator ϵ is the symmetric part of the gradient operator, while the divergence operator, div, is applied row–wise on matrix valued functions. Finally, J denotes the second order operator obtained by first taking curl of each row, followed by applying the curl operator to each column. This operator maps $C^\infty(\mathbb{S})$ into itself.

In [2] it is described how the elasticity complex is connected to the de Rham complex via the Bernstein–Gelfand–Gelfand resolution. In this talk we discuss how we can obtain discrete elasticity complexes, from known discrete de Rham complexes, by mimicking the Bernstein–Gelfand–Gelfand procedure in the discrete case. As a result, new and simple mixed elasticity elements are constructed. In particular, for the mixed finite element formulation with weakly imposed symmetry, as in [1], we construct stable elements consisting of only piecewise linear stresses, and piecewise constant displacements. These finite element spaces appear to be simpler than those proposed previously.

References

[1] Douglas N. Arnold, Franco Brezzi, and Jim Douglas, Jr., *PEERS: a new mixed finite element for plane elasticity*, Japan J. Appl. Math. **1** (1984), no. 2, 347–367.
[2] Michael Eastwood, *A complex from linear elasticity*, Rend. Circ. Mat. Palermo (2) Suppl. (2000), no. 63, 23–29.

Finite element methods for nearly incompressible elasticity based on Hu-Washizu formulation

Barbara I. Wohlmuth
(joint work with J. K. Djoko, B. P. Lamichhane and B. D. Reddy)

The classical three-field Hu-Washizu mixed formulation for problems in elasticity is examined afresh through a modified formulation, with the emphasis on behavior in the incompressible limit. This new formulation is parameterized by a scalar α, with $\alpha = 1$ corresponding to the standard Hu-Washizu formulation. It is shown that, provided that $\alpha \neq -\mu/\lambda$, where μ and λ are the Lamé parameters in elasticity, the continuous problem has a unique solution, with α- and λ-independent bounds on the solution. Finite element approximations on planar domains are considered, in which the displacements are approximated on quadrilaterals by piecewise-bilinear functions. For these classes of discrete problems, conditions for uniform convergence are made explicit. These conditions are shown to be met by particular choices of approximations based on quadrilateral elements, and include bases that are well-known as well as newly constructed bases.

The standard Hu-Washizu formulation is obtained by considering the constitutive equation, the strain-displacement equation and the equation of equilibrium in a weak form. For the linear elastic body in $\Omega \subset \mathbb{R}^2$, the modified

formulation depending on $\alpha := \alpha(\mu, \lambda)$ considered in in [5] is given by: find $(\boldsymbol{u}_h, \boldsymbol{d}_h, \boldsymbol{\sigma}_h) \in V_h \times D_h \times S_h \subset H^1(\Omega)^2 \times L^2(\Omega)^{2\times 2} \times L^2(\Omega)^{2\times 2}$ such that

$$a_\alpha((\boldsymbol{u}_h, \boldsymbol{d}_h), (\boldsymbol{v}_h, \boldsymbol{e}_h)) + b_\alpha((\boldsymbol{v}_h, \boldsymbol{e}_h), \boldsymbol{\sigma}_h) \quad = \ell(\boldsymbol{v}_h), \quad (\boldsymbol{v}_h, \boldsymbol{e}_h) \in V_h \times D_h,$$

$$b_\alpha((\boldsymbol{u}_h, \boldsymbol{d}_h), \boldsymbol{\tau}_h) \quad - \frac{(1-\alpha)\lambda}{4(\mu+\lambda)^2} \, c(\boldsymbol{\sigma}_h, \boldsymbol{\tau}_h) = 0, \quad \boldsymbol{\tau}_h \in S_h,$$

where the bilinear forms are defined by

$$a_\alpha((\boldsymbol{u}_h, \boldsymbol{d}_h), (\boldsymbol{v}_h, \boldsymbol{e}_h)) := 2\mu(\boldsymbol{d}_h, \boldsymbol{e}_h)_0 + \alpha\lambda(\operatorname{tr}\boldsymbol{d}_h, \operatorname{tr}\boldsymbol{e}_h)_0,$$

$$b_\alpha((\boldsymbol{v}_h, \boldsymbol{e}_h), \boldsymbol{\sigma}_h) := (\boldsymbol{\varepsilon}(\boldsymbol{v}_h) - 2\mu\,\mathcal{C}^{-1}\boldsymbol{e}_h, \boldsymbol{\sigma}_h)_0 - \frac{\alpha\lambda}{2(\mu+\lambda)}(\operatorname{tr}\boldsymbol{\sigma}_h, \operatorname{tr}\boldsymbol{e}_h)_0,$$

$$c(\boldsymbol{\sigma}_h, \boldsymbol{\tau}_h) := (\operatorname{tr}\boldsymbol{\sigma}_h, \operatorname{tr}\boldsymbol{\tau}_h)_0.$$

Utilizing the Voigt notation, the spaces S_h and D_h are generated from bases $S_\square$ and $D_\square$ defined on $\hat{K} := (-1,1)^2$. Defining

$$\mathcal{I} := \operatorname{span}\begin{bmatrix} 1 & 0 & 0 \\ 0 & 1 & 0 \\ 0 & 0 & 1 \end{bmatrix}, \ A := \operatorname{span}\begin{bmatrix} \hat{y} & 0 \\ 0 & \hat{x} \\ 0 & 0 \end{bmatrix}, \ B := \operatorname{span}\begin{bmatrix} \hat{x} & 0 \\ 0 & \hat{y} \\ 0 & 0 \end{bmatrix}, \ C := \operatorname{span}\begin{bmatrix} 0 & 0 \\ 0 & 0 \\ \hat{x} & \hat{y} \end{bmatrix},$$

some interesting choices of (S_h^i, D_h^i), $1 \le i \le 5$ are:

TABLE 2. Different cases for the discrete spaces

Case	I	II	III	IV	V
$S_\square$	$\mathcal{I} + A$	$\mathcal{I} + A$	$\mathcal{I} + C$	$\mathcal{I} + A + C$	$\mathcal{I} + A + C$
$D_\square$	$\mathcal{I} + A$	$\mathcal{I} + A + B$	$\mathcal{I} + C$	$\mathcal{I} + A + C$	$\mathcal{I} + A + B + C$
	$S_h^1 = D_h^1$	$S_h^2 \subset D_h^2$	$S_h^3 = D_h^3$	$S_h^4 = D_h^4$	$S_h^5 \subset D_h^5$

Case II corresponds to the method of mixed enhanced strains [3, 4] while Case V corresponds to the method of enhanced assumed strains [6].

While the spherical part of the stress might be polluted by checkerboard modes, as in the case of the $Q_1 - P_0$ element, see also [2], it is shown in [5] that the error in displacement satisfies a λ-independent a priori error estimate, and an optimal a priori error estimate for the post-processed stress is established. The degrees of freedom corresponding to stresses and strains are defined only element-wise, and can easily be condensed out from the system. The theoretical analysis is carried out for this statically condensed displacement-based formulation. Since the discrete solutions for Cases I and IV depend on α, explicit bounds on α are presented for the λ-independent error estimates.

Numerical Results:

We illustrate the performance of the formulation for isotropic and nearly incompressible materials in plane strain, in two numerical tests. The implementation is based on the finite element toolbox UG, [1].

Example 1: Cook's membrane problem

In this popular benchmark problem [6, 3], we set $\Omega := \operatorname{conv}\{(0,0), (48,44), (48,60), (0,44)\}$, where $\operatorname{conv}\xi$ is the convex hull of the set ξ. The left boundary of the tapered panel Ω is clamped, and the right one is subjected to an in-plane shearing load of 100N
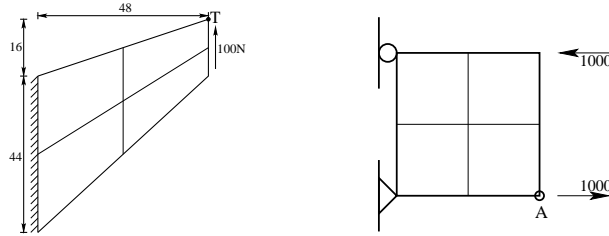
FIGURE 1. (a) Cook's membrane problem with initial triangulation; (b) the square beam problem with a mesh of four squares

along the y-direction, as shown in Figure 1(a). The material properties are taken to be $E = 250$ and $\nu = 0.4999$, so that a nearly incompressible response is obtained.

The vertical tip displacement at the point T is computed for the different cases in Table 2, for different levels of uniform refinement, starting with the initial triangulation shown in Figure 1 (a). As can be seen from Table 3, the standard displacement approach and standard Hu-Washizu formulation ($\alpha = 1$) with stress and strain spaces given in Cases I and IV exhibit locking whereas all other cases show rapid convergence.

TABLE 3. Vertical tip displacement at point T, Example 1

	$\alpha = 1$		α independent			$\alpha = \frac{\mu}{4\lambda}$		$\alpha = -\frac{\mu}{4\lambda}$		$\alpha = 0$		Q_1-P_0
lev	Q_1	I	II	III	V	I	IV	I	IV	I	IV	
0	2.00	2.00	4.00	4.58	3.15	2.93	2.70	3.18	2.82	3.04	2.75	3.01
1	2.07	2.08	5.40	5.64	4.42	4.18	3.76	4.53	3.97	4.34	3.86	4.31
2	2.10	2.12	6.73	7.02	6.24	5.93	5.60	6.20	5.83	6.06	5.71	6.28
3	2.15	2.22	7.59	7.52	7.17	7.00	6.85	7.13	6.97	7.06	6.91	7.21
4	2.32	2.54	7.59	7.68	7.53	7.45	7.40	7.50	7.45	7.48	7.42	7.55
5	2.84	3.39	7.69	7.73	7.67	7.63	7.62	7.66	7.64	7.64	7.63	7.68
6	4.03	4.94	7.74	7.75	7.73	7.71	7.70	7.72	7.71	7.71	7.71	7.73

Example 2: Square beam

In the second example, we illustrate the dependence of the numerical solution $\boldsymbol{u}_h$ on α. Here, we consider the domain $\Omega := (0, 2) \times (0, 2)$, which is fixed in the x-direction at the point $(0, 2)$ and fixed in both directions at the origin. A linearly varying horizontal force is applied in the x-direction along the boundary $x = 2$, with resultant point forces $p = 1000$ at $(2, 0)$ and $p = -1000$ at $(2, 2)$ (Figure 1 (b)).

In Figure 2 the absolute error of the vertical tip displacement at A versus $\frac{\alpha\lambda}{2\mu}$ has been shown. The left picture shows the Case IV and the right pictures shows the Case I with $E = 1500$ and $\nu = 0.4999$. As can be seen from Figure 2, the locking effect increases with $\alpha\lambda$, and the optimal α is negative.
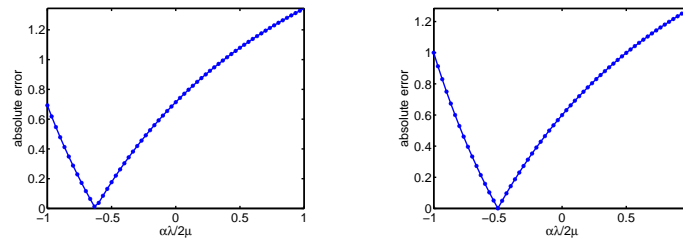
FIGURE 2. Error of the vertical tip displacement at A versus $\frac{\alpha\lambda}{2\mu} \in$ $[-1, 1]$, Case IV (left) and Case I (right)

REFERENCES

[1] P. Bastian, K. Birken, K. Johannsen, S. Lang, N. Neuß, H. Rentz–Reichert, and C. Wieners. UG – a flexible software toolbox for solving partial differential equations. *Computing and Visualization in Science*, 1:27–40, 1997.

[2] D. Braess, C. Carstensen, and B.D. Reddy. Uniform convergence and a posteriori error estimators for the enhanced strain finite element method. *Numer. Math.*, 96:461–479, 2004.

[3] E.P. Kasper and R.L. Taylor. A mixed-enhanced strain method. Part I: geometrically linear problems. *Comp. Struct.*, 75:237–250, 2000.

[4] E.P. Kasper and R.L. Taylor. A mixed-enhanced strain method. Part II: geometrically non-linear problems. *Comp. Struct.*, 75:251–260, 2000.

[5] B.P. Lamichhane, B.D. Reddy, and B.I. Wohlmuth. Convergence in the incompressible limit of finite element approximations based on the hu-washizu formulation. Technical Report 05, University of Stuttgart, SFB 404, 2004.

[6] J.C. Simo and M.S. Rifai. A class of assumed strain methods and the method of incompatible modes. *Int. J. Numer. Meth. Engrg.*, 29:1595–1638, 1990.

Reporter: Carsten Carstensen

Participants

Prof. Dr. Mark Ainsworth
m.ainsworth@strath.ac.uk
Department of Mathematics
University of Strathclyde
Livingstone Tower
26, Richmond Street
GB-Glasgow, G1 1XH

Todd Arbogast
arbogast@math.utexas.edu
Department of Mathematics
University of Texas at Austin
1 University Station C1200
Austin, TX 78712-1082
USA

Prof. Dr. Francisco Armero
armero@ce.berkeley.edu
Structural Eng., Mech. and Material
Dept. of Civil and Envirom. Eng.
Univ. of California, Berkeley
721 Davis Hall
Berkeley CA 94720-1710
USA

Dr. Sören Bartels
sba@math.hu-berlin.de
Institut für Mathematik
Humboldt-Universität zu Berlin
Unter den Linden 6
10099 Berlin

Prof. Dr. Roland Becker
roland.becker@univ-pau.fr
Laboratoire de Mathematiques
Appliquees
Universite de Pau et des Pays de
l'Adour, BP 1155
F-64013 Pau Cedex

Prof. Dr. Kai-Uwe Bletzinger
kub@bv.tum.de
Lehrstuhl für Statik
Technische Universität
Arcisstr. 21
80333 München

Prof. Dr. Dietrich Braess
braess@num.ruhr-uni-bochum.de
Fakultät für Mathematik
Ruhr-Universität Bochum
44780 Bochum

Prof. Dr. Susanne C. Brenner
brenner@math.sc.edu
Dept. of Mathematics
University of South Carolina
Columbia, SC 29208
USA

Prof. Dr. Carsten Carstensen
cc@math.hu-berlin.de
Institut für Mathematik
Humboldt-Universität zu Berlin
Unter den Linden 6
10099 Berlin

Prof. Dr. Ricardo Duran
rduran@mate.dm.uba.ar
rduran@dm.uba.ar
Dto. de Matematica - FCEYN
Universidad de Buenos Aires
Ciudad Universitaria
Pabellon 1
1428 Buenos Aires
ARGENTINA

Prof. Dr. Richard S. Falk
falk@math.rutgers.edu
Department of Mathematics
RUTGERS University
Hill Center, Busch Campus
110 Frelinghuysen Road
Piscataway, NJ 08854-8019
USA

Dr. Stefan A. Funken
stefan.funken@brunel.ac.uk
BICOM and School of Information
Systems, Computing and Mathematics
Brunel University
Uxbridge
GB-Middlesex UB8 3PH

Prof. Dr. Krishna Garikipati
krishna@umich.edu
Department of Mechanical Engineer.
University of Michigan, College of
Engineering, 2350 Hayward
2250 GG Brown
Ann Arbor MI 48109-2125
USA

Prof. Dr. Wolfgang Hackbusch
wh@mis.mpg.de
Max-Planck-Institut für Mathematik
in den Naturwissenschaften
Inselstr. 22 - 26
04103 Leipzig

Prof. Dr. Klaus Hackl
hackl@am.bi.ruhr-uni-bochum.de
Lehrstuhl für Allgemeine Mechanik
Ruhr-Universität Bochum
Fakultät für Bauingenieurwesen
44780 Bochum

Dr. Peter Hansbo
hansbo@am.chalmers.se
Department of Applied Mechanics
Chalmers University of Technology
and University of Göteborg
Sven Hultins gata 6
S-41296 Göteborg

Prof. Dr. Ronald H.W. Hoppe
hoppe@math.uni-augsburg.de
rohop@math.uh.edu
Lehrstuhl für Angewandte
Mathematik I
Universität Augsburg
Universitätsstr. 14
86159 Augsburg

Dr. Ulrich Hoppe
hoppe@am.bi.ruhr-uni-bochum.de
Lehrstuhl für Allgemeine Mechanik
Ruhr-Universität Bochum
Fakultät für Bauingenieurwesen
Universtitätsstr. 150
44801 Bochum

Prof. Paul Houston
paul.houston@mcs.le.ac.uk
Department of Mathematics
University of Leicester
University Road
GB-Leicester, LE1 7RH

Dr. Jun Hu
hujun@mathematik.hu-berlin.de
c/o Prof. Dr. Carsten Carstensen
Institut für Mathematik
Humboldt-Universität zu Berlin
Unter den Linden 6
10099 Berlin

Isidora Ivljanin
ivljanin@am.bi.rub.de
Lehrstuhl für Allgemeine Mechanik
Ruhr-Universität Bochum
44780 Bochum

Dr. Max Jensen
jensenm@math.hu-berlin.de
Institut für Mathematik
Humboldt-Universität zu Berlin
Unter den Linden 6
10099 Berlin

Prof. Dr. Peter Knabner
knabner@am.uni-erlangen.de
Inst. für Angewandte Mathematik 1
Universität Erlangen
Martensstr. 3
91058 Erlangen

Prof. Dr. Ulrich Langer
ulanger@numa.uni-linz.ac.at
Institut für Numerische Mathematik
Johannes Kepler Universität Linz
Altenbergstr. 69
A-4040 Linz

Prof. Dr. Rajco D. Lazarov
lazarov@math.tamu.edu
Department of Mathematics
Texas A & M University
College Station, TX 77843-3368
USA

Prof. Dr. Carlo Lovadina
carlo.lovadina@unipv.it
Dipartimento di Matematica
Universita di Pavia
Via Ferrata 1
I-27100 Pavia

Julia Mergheim
mergheim@rhrk.uni-kl.de
Lehrstuhl für Techn. Mechanik
T.U. Kaiserslautern
Erwin-Schrödinger-Straße
67663 Kaiserslautern

Prof. Dr. Christian Miehe
Miehe@mechbau.uni-stuttgart.de
em@mechbau.uni-stuttgart.de
Institut für Mechanik (Bauwesen)
Universität Stuttgart
70550 Stuttgart

Prof. Dr. Peter Monk
monk@math.udel.edu
Department of Mathematical Sciences
University of Delaware
501 Ewing Hall
Newark, DE 19716-2553
USA

Dr. Florin Adrian Radu
raduf@am.uni-erlangen.de
Mathematisches Institut
Universität Erlangen-Nürnberg
Bismarckstr. 1 1/2
91054 Erlangen

Prof. Dr. Rolf Rannacher
rannacher@iwr.uni-heidelberg.de
rolf.rannacher@iwr.uni-heidelberg.de
Institut für Angewandte Mathematik
Universität Heidelberg
Im Neuenheimer Feld 294
69120 Heidelberg

Prof. Dr. B. Daya Reddy
bdr@maths.uct.ac.za
bdr@science.uct.ac.za
University of Cape Town
Faculty of Science
Private Bag
7701 Rondebosch
South Africa

Prof. Dr. Stefanie Reese
reese@nm.ruhr-uni-bochum.de
Ruhr-Universität Bochum
Fakultät für Bauingenieurwesen
AG Numerische Mechanik + Simulation
Gebäude IA 01/128
44780 Bochum

Prof. Dr. Riccardo Sacco
riccardo.sacco@mate.polimi.it
Dipartimento di Matematica
Politecnico di Milano
Piazza Leonardo da Vinci, 32
I-20133 Milano

Dr. Joachim Schöberl
js@jku.at
Institut für Mathematik
Universität Linz
Altenberger Str. 69
A-4040 Linz

Prof. Dr.Dr.h.c. Erwin Stein
stein@ibnm.uni-hannover.de
Institut für Baumechanik und
Numerische Mechanik
Universität Hannover
Appelstr. 9A
30167 Hannover

Prof. Dr. Paul Steinmann
ps@rhrk.uni-kl.de
Lehrstuhl für Techn. Mechanik
T.U. Kaiserslautern
67653 Kaiserslautern

Prof. Dr. Ernst Peter Stephan
stephan@ifam.uni-hannover.de
Institut für Angewandte Mathematik
Universität Hannover
Welfengarten 1
30167 Hannover

Prof. Dr. Rüdiger Verfürth
rv@num1.ruhr-uni-bochum.de
Fakultät für Mathematik
Ruhr-Universität Bochum
44780 Bochum

Prof. Dr. Werner Wagner
ww@bs.uka.de
Institut für Baustatik
Universität Karlsruhe (TH)
Kaiserstrasse 12
76131 Karlsruhe

Prof. Dr.Ing. Wolfgang A. Wall
wall@lnm.mw.tum.de
Lehrstuhl für Numerische Mechanik
Technische Universität München
Boltzmannstraße 15
85748 Garching bei München

Dr. Kerstin Weinberg
kerstin.weinberg@tu-berlin.de
Technische Universität Berlin
Institut für Mechanik Sekr. MS 2
FG Kontinuumsmechanik u. Materilth.
Einsteinufer 5
10587 Berlin

Prof. Dr. Christian Wieners
wieners@math.uni-karlsruhe.de
Institut für Praktische Mathematik
Universität Karlsruhe
76128 Karlsruhe

Prof. Dr. Ragnar Winther
ragnar.winther@cma.uio.no
Centre of Mathematics for
Applications
University of Oslo
P.O. Box 1053, Blindern
N-0316 Oslo 3

Prof. Dr. Barbara Wohlmuth
wohlmuth@mathematik.uni-stuttgart.de
Mathematisches Institut A
Universität Stuttgart
Pfaffenwaldring 57
70569 Stuttgart